CHEMICAL ENGINEERING SCIENCE
GENIE CHIMIQUE

VOL. 6 MARCH 1957 No. 3

The selective behaviour of ion-exchange membranes at high concentrations

G. G. MADGWICK

School of Chemical Engineering, The N.S.W. University of Technology, Kensington, N.S.W., Australia

(*Received* 1 *August* 1956)

Abstract—The selective properties of the ion-permeable membranes " Permaplex A-10 " and " Permaplex C-10 " in concentrated sodium-chloride solutions have been studied. Transport numbers have been obtained as a function of the mean concentration and concentration ratio existing outside the membranes. For a given mean concentration, both membranes show higher selectivity for high concentration ratios. Membrane transport numbers approach 0·6 at saturation.

It has been shown that a three compartment cell, operating under special conditions, may demonstrate the true selectivity of the membranes. Back diffusion of electrode products was limited by high flow rates and short running times. Current efficiencies fall below those predicted from transport numbers, largely due to electro-osmosis, and are less than 20% at saturation.

Résumé—L'auteur étudie les proriétés sélectives des membranes semi-perméables " Permaplex A-10 " et " Permaplex C-10 " dans des solutions concentrées de chlorure de sodium. Il a obtenu les nombres de transfert en fonction de la concentration moyenne et du rapport des concentrations à l'extérieur des membranes. Pour une concentration moyenne donnée, les deux membranes montrent une sélectivité plus grande pour des rapports de concentration élevés. A la saturation, les nombres de transfert s'approchent de 0·6.

L'auteur montre qu'avec une cellule à trois compartiments travaillant dans des conditions déterminées, on peut mettre en évidence la séléctivité réelle des membranes. Grâce à des vitesses d'écoulement rapides et des durées suffisamment courtes, on peut alors limiter la diffusion en retard des produits aux électrodes. Les rendements en courant descendent au-dessous des valeurs prévues à partir des nombres de transport, en grande partie à cause de l'éctro-osmose. A la saturation, ils sont réduits de 20%.

1. INTRODUCTION

THE present research was undertaken to determine the feasibility of applying ion-exchange membranes as separating media in concentrated brine solutions. The " Permutit " membranes used are typical of the few types now produced. They combine a high degree of selectivity with minimum electrical resistance and will thus give maximum separation with minimum power usage. The experiments were therefore undertaken for the final purpose of making design estimates for a large-scale, multicompartment separating unit, and the apparatus necessarily had to reproduce conditions analogous to those within such a cell.

The general properties of ion-permeable membranes and the theory of their operation have been widely discussed and will not be repeated here. SOLLNER [15] has given many references to earlier work on membrane preparation and theory.

Commercial membranes of the type used in this research have been described by JUDA and MCRAE [9], KRESSMAN [11], WINGER *et al.* [20] and " Anon." [2]. Technical data on the the membranes " Permaplex C-10 " and

"Permaplex A-10" have been given by the Permutit Co. Ltd. [13]. These commercial membranes have been used both for analytical and laboratory purposes (WILLARD and FINLEY [19], FRISCH [3, 4, 5], ANDERSON and WYLAM [1], SHAIR *et al.* [14], and KUNIN [12]) and for desalting in multicompartment cells (WINGER *et al.* [21] WALTERS, WEISER and MAREK [17], WIECHERS and VAN HOEK [18], and Ionics Incorporated [8]).

2. EXPERIMENTAL

(a) *Membrane transport numbers*

The transport numbers of the selected ion in "Permaplex C-10" and "Permaplex A-10" were computed from concentration potentials existing across the membranes when separating solutions of different activity.

Consideration of molar free-energy changes involved in such a cell leads to the expression

$$E = RT/F\,(2t_{\pm} - 1) \ln a_1^{\pm}/a_2^{\pm} \qquad (1)$$

where

E = membrane potential
F = Faraday constant
$t_{\pm}$ = transport number of selected ion
a_1, a_2 = mean ionic activities in solutions 1 and 2

The theoretical maximum value of the concentration potential is given by

$$E_0 = RT/F \ln a_1^{\pm}/a_2^{\pm}. \qquad (2)$$

Thus

$$t_{\pm} = (E_0 + E)/2E_0. \qquad (3)$$

Equation (3) gives an average transport number in the range $a_1 + a_2$. If the activities of the solutions surrounding the membrane are almost equal, $t_{\pm}$ may be assumed linear in $\ln a_1, a_2$ and will then be a function of the geometric mean of a_1 and a_2. Other investigators have used various parameters to express concentration. SOLLNER [15] used the upper concentrations with 2/1 ratio. WINGER, BODAMER and KUNIN [20] used the arithmetic mean concentration with the same ratio. JUDA *et al.* [10] have used a ratio of 2/1 and plotted transport numbers against geometric mean concentration. For this work an arithmetic mean was arbitrarily chosen, since such a plot will reveal whether the concentration gradient through the membrane is linear for various external-concentration ratios.

(i) *Procedure.* Membrane potentials were measured in a flow cell of the type given below:

Hg/Hg_2Cl_2	Sat. KCl Agar	Solution M_1	Membrane	Solution M_2	Sat. KCl Agar	Hg/Hg_2Cl_2

The cell was made in two halves from welded polyethylene, and assembled with the membrane between, acting as its own gasket. The solutions in use were fed at a rate of 30 ml/min to give a complete volume change in under one minute. Potential measurements were made using a Leeds and Northrup type 7552 potentiometer (K-2) with a galvanometer type 2430 of the same make. When two consecutive readings taken at intervals of one minute agreed within 0·05 mV, the potentiometer reading was taken as the concentration potential under the conditions applied. The symmetry of the electrodes was checked before and after every potential measurement. Readings were made at a temperature of 25·0C, with arithmetic mean concentration values ranging from 0·06 molar to 2.88 molar. The molarity ratios studied were 2, 4, 8, and 20 to 1.

(ii) *Results.* The transport numbers for the sodium ion in "Permaplex C-10" and chloride ion in "Permaplex A-10" are plotted in Fig. 1 and 2 as a function of the arithmetic mean concentration. Figs. 3 and 4 show transport numbers as a function of concentration ratio and indicate how the curves for a 1/1 ratio were obtained (see Figs. 1 and 2).

Activity data were taken from HARNED and OWEN [7] and the data for the saturation line in Figs. 1 and 2 from *Handbook of Chemistry and Physics* [6].

(b) *Three-compartment membrane cell*

The three-compartment cell is the simplest unit demonstrating the properties of both anion and cation selective membranes. FRISCH [3] used the cell for electrolytic precipitation of uranium. ANDERSON and WYLAM [1] demineralized sugar

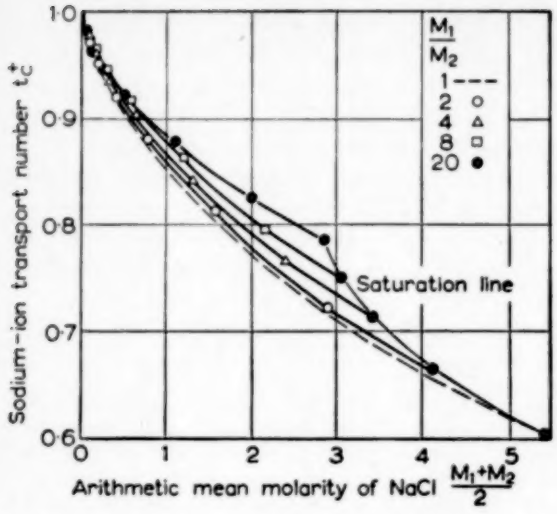

FIG. 1. Transport number of sodium ion in Permaplex C-10.

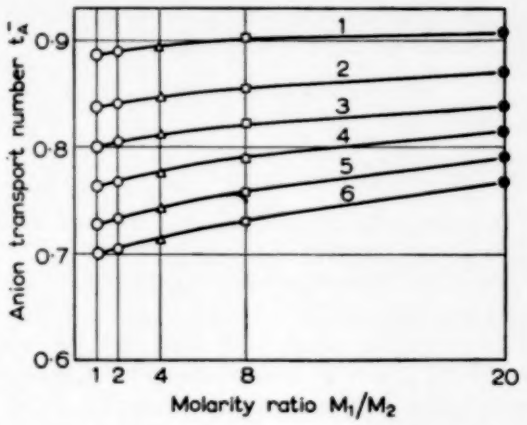

FIG. 3. The effect of concentration ratio on cation transport through Permaplex C-10.

(1) 0·5 Molar
(2) 1·0 Molar
(3) 1·5 Molar
(4) 2·0 Molar
(5) 2·5 Molar
(6) 3·0 Molar

solutions in a three-compartment cell with "Permaplex" membranes, while WILLARD and FINLEY [19] used a similar cell for separation of uranium tetrafluoride. WALTERS, WEISER and MAREK [17] proposed placing ion-exchange resin between the membranes of a three compartment cell to obtain decontamination of radioactive wastes.

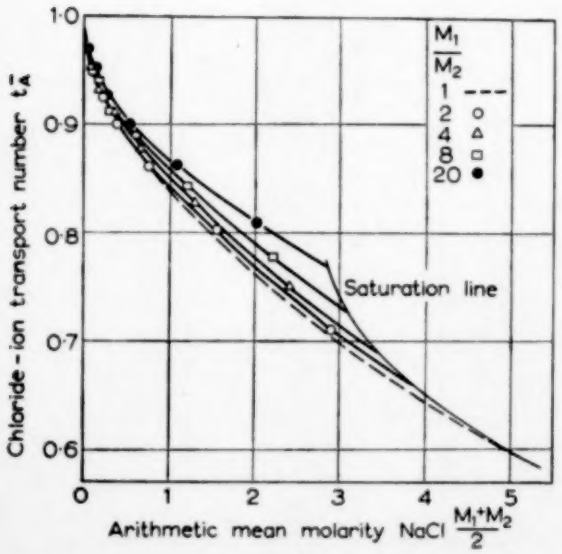

FIG. 2. Transport number of chloride ion in Permaplex A-10.

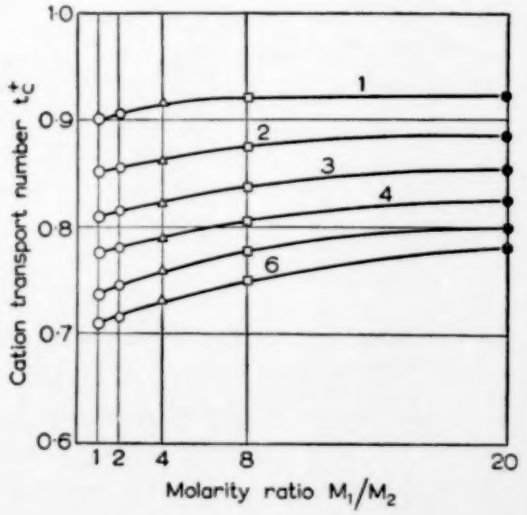

FIG. 4. The effect of concentration ratio on anion transport through Permaplex A-10.

(1) 0·5 Molar
(2) 1·0 Molar
(3) 1·5 Molar
(4) 2·0 Molar
(5) 2·5 Molar
(6) 3·0 Molar

Mass transfer occurs through ion-permeable membranes by four mechanisms :

(i) normal electrodialysis,
(ii) ionic diffusion,
(iii) osmosis,
(iv) electro-osmosis.

Transfer by mechanism (i) may be predicted from the membrane selectivity :

Consider a three-compartment cell containing in all parts a solution of the monovalent salt MX. (The various compartments need not contain solutions of equal strength). The centre compartment is bounded by a cation membrane on the cathode side and an anion-permeable membrane on the other. A potential is applied to the system through suitable electrodes in the outer compartments.

In a given time interval let M^+ cations pass through the cation membrane towards the cathode. At the same time x^- ions will pass in the opposite direction due to the imperfect nature of the membrane. Also in this time interval, let X^- anions pass towards the anode and m^+ ions in the opposite direction.

The efficiency of the cation membrane

$$\eta_c = \frac{\text{net ions passed to catholyte}}{\text{total ions transferred}}$$

$$= \frac{M^+ - x^-}{M^+ + x^-}$$

which by inspection

$$= \frac{t_c^+ - t_c^-}{t_c^+ + t_c^-}$$

$$= 2t_c^+ - 1$$

where

t_c^+ = transport number of cation in cation selective membrane

t_c^- = transport number of anion in cation selective membrane.

Similarly, the efficiency of the anion membrane

$$\eta_A = 2t_A^- - 1.$$

The cell efficiency is the arithmetic mean of η_c and η_A

$$\eta_{\text{cell}} = (t_c^+ + t_A^-) - 1.$$

This efficiency, which ignores mechanisms (ii), (iii), and (iv), will in general be different from that of a real membrane under operating conditions. Diffusion and osmosis have an additive effect equivalent to a net transfer of solute from concentrated to dilute solution adjacent to the membrane. In a three-compartment cell, electro-endosmosis and electro-osmosis cause solvent transfer towards the electrodes at a rate dependent on ambient concentration, applied potential, and the distribution of charged groups in the membrane.

(I) *Apparatus.* The three-compartment cell used is shown in Fig. 5. The electrode chambers were machined from methacrylate plastic, with cemented joints. The centre compartment spacer was cut from polythene 3 mm thick and was baffled to give six passes across the membrane face, and excellent mixing throughout the compartment. (Flow patterns in the compartment were examined by dye injection before a final baffle layout was made.) The cell had an overall diameter of 20 cm and a free membrance area of 100 sq. cm. Liquid holdup was kept low and was about 25 ml for the centre and

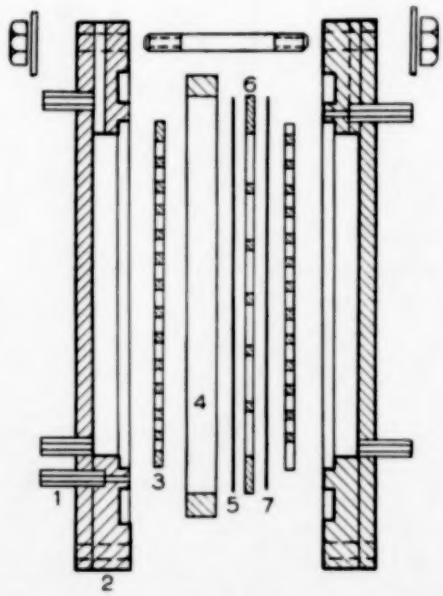

Fig. 5. Sectional exploded view of three-compartment cell.

(1) Solution feed
(2) End compartment
(3) Membrane support
(4) Locating ring
(5) Anion membrane
(6) Centre compartment
(7) Cation membrane

100 ml for the electrode compartments. By placing a perforated support plate outside the membranes and a positive pressure in the centre compartment, disturbance of the membranes during operation was avoided. Power was supplied from a rotary d.c. generator to graphite electrodes of face area 80 sq. cm. Conventional rheostat control with voltmeter, ammeter, and a copper coulometer was provided.

A flow diagram of the arrangement is shown in Fig. 6. Originally it was intended to run the electrode feeds at high rates and to follow the change in concentration of the recycled centre stream with a flow-type conductivity cell (Philips-type G.M. 4247, bridge-type G.M. 4249). This system was unsuitable since during a running time of 30-60 min the back diffusion of electrode products (i.e. H_3O^+ and OH^- ions) caused *p*H changes which, although not significant in terms of ionic transfer, had a

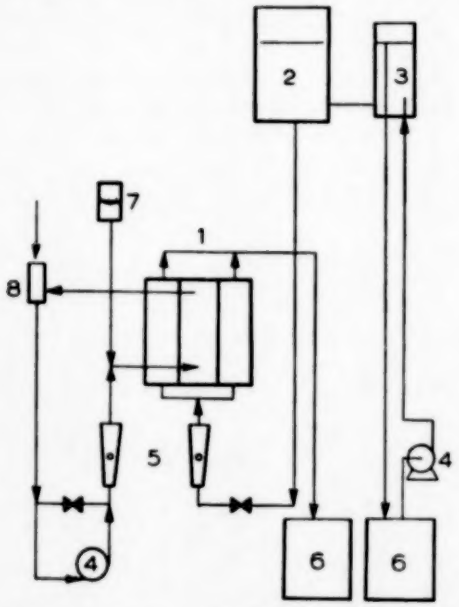

Fig. 6. Flow diagram of three-compartment cell.

(1) Cell	(5) Flow meter
(2) Electrode feed	(6) Solution storage
(3) Head tank	(7) Pulsation damper
(4) Pump	(8) Centre feed

marked effect on conductivity. Also at high concentrations the conductivity bridge became insensitive because of the presence of stray potentials and earthing problems. Difficulty was experienced in circulating the small volume of solution through the centre compartment, and a special roller pump (operating by squeezing the liquid through a rubber tube) was developed for the purpose.

The final experimental method called for very short runs – 10-20 minutes. A constant current of four amps (3·72 amps correct) was used rather than constant voltage, because of its greater significance in determining rate of transfer, and because it facilitated interpretation of results. The centre compartment flow rate was also kept approximately constant at 40 ml/min. (It has been found (author, unpublished data), that the rate of material transfer through the membrane is independent of flow rate in a cell of this type where the Reynolds number in the compartments is greater than about 500.)

(II) *Procedure.* The electrode streams were started and maintained at 1000 ml/min (500 ml per electrode). The centre compartment system was rinsed with distilled water, purged with compressed air, and 100 ml of solution of approximately correct concentration was added through the feed opening. After circulating for about two minutes a 25-ml sample was withdrawn for analysis, and the power was switched on. At the end of the run, the power was cut, and the whole contents of the centre stream were blown into a suitable receiver.

Analysis of the centre stream was achieved by evaporating a 3-ml sample in a deep glass weighing bottle in an oven at 150°C, drying for a further four hours and weighing.

A total of 133 runs was carried out in the cell, covering a range of concentration in both streams of about 3-29 per cent (wt./vol.). The runs were arbitrarily grouped by maintaining a fixed electrode stream concentration for a series of about twelve centre-compartment strengths. 1-28 were conductivity monitored and were rejected. Runs 29-50 and 78-90 were also rejected because of leakage. Both membranes were replaced after run 90, with no apparent effect on the results. Because of the nature of the equipment, it was inconvenient to maintain a controlled temperature, but at all times the operating temperatures fell within the range 23-26°C. The short running time for each test and the rather complex nature of the centre-stream system made impractical direct measurement of volume change due to solvent transfer.

(iii) *Results.* Cell-current efficiencies, and efficiencies calculated from transport-number data are shown in Figs. 7, 8, 9 and 10.

3. Discussion

(a) *Transport numbers*

The results show that, for a given arithmetic mean concentration, a high concentration ratio will result in a correspondingly increased transport number for the selected ion within the membrane. This indicates that, except at low concentration differences (say up to 2/1 ratio), the concentration gradient between the membrane faces is not linear. Replotting Figs. 1 and 2 in terms of geometric means or even mean activities does not result in a single relationship for the experimental data.

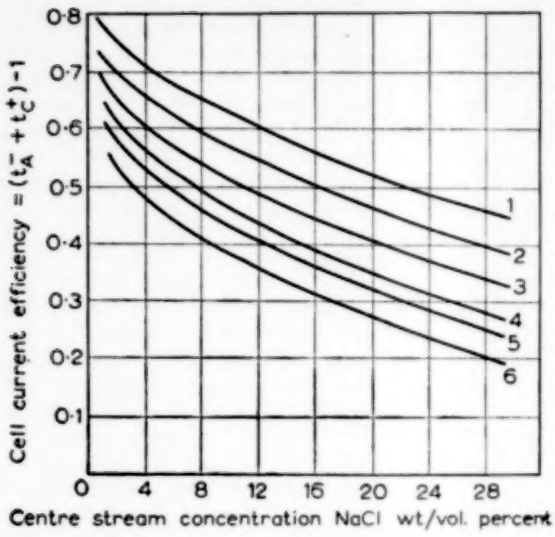

FIG. 7. Cell-current efficiency computed from transport numbers. Electrode-stream concentration wt./vol. per cent.

(1) 5·2	(4) 19·0
(2) 9·1	(5) 22·8
(3) 14·5	(6) 28·8

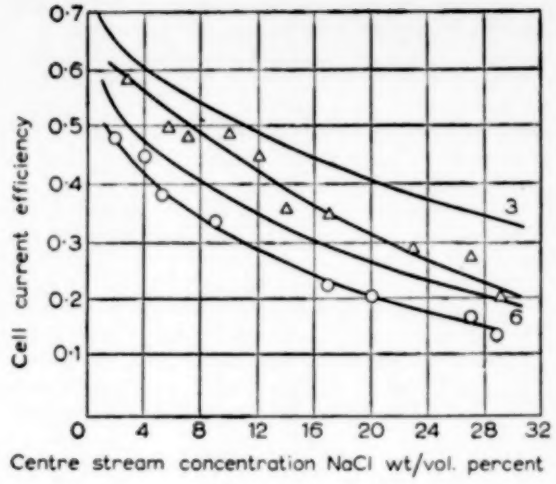

FIG. 9. Experimental 3-compartment-cell efficiency. Electrode-stream concentration Wt./vol. per cent.

	Measured	Fig. 7
14·5	△	(3)
28·8	○	(6)

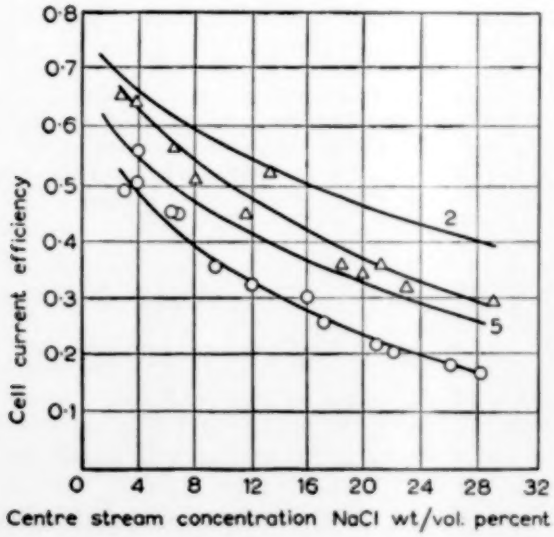

FIG. 8. Electrode-stream concentration Wt./vol. per cent.

	Measured	Fig. 7
9·1	△	(2)
22·8	○	(5)

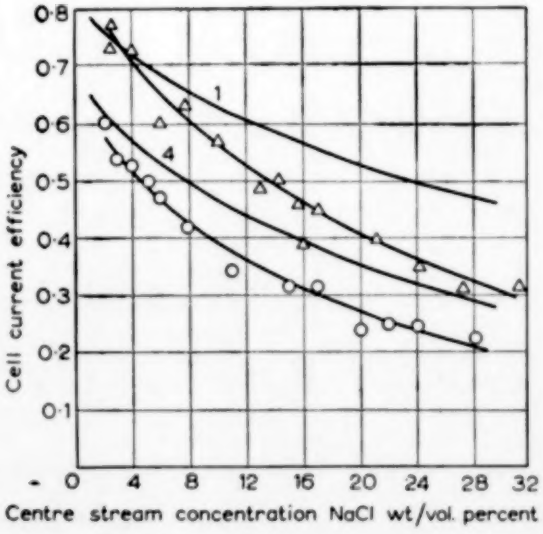

FIG. 10. Experimental 3-compartment cell efficiency. Electrode-stream concentration Wt./vol. per cent.

	Measured	Fig. 7
5·15	△	(1)
19·0	○	(4)

Since the transport numbers are measured indirectly in terms of a balanced potential value, they may be considered independent of any net electro kinetic transfer across the membrane. However with high concentration differences the osmotic driving force tending to cause solvent transfer will be greater, and, even considering the very low hydraulic permeability of these commercial membranes, it would be possible for solvent ingress (independent of that associated with the charged layer near the active resin groups) to result in a decreased equilibrium concentration within the membrane. As can be seen from the figures, a measurement of transport numbers at a concentration ratio of 2/1, as has been accepted practice for most investigators, is insignificantly different from the ideal condition developed by extrapolation.

The precautions taken to obtain these highly reproducible results have been outlined by Sollner and Gregor [16].

(b) *Three-compartment cell*

Efficiencies obtained with the three-compartment cell were lower than indicated by transport numbers at all the concentrations studied. This resulted from material transfer by mechanisms other than simple electrodialysis. Electro-osmosis, which would cause solvent transfer from the centre to the electrode compartments, should cause an apparent efficiency decrease. Osmosis and diffusion may either improve or impair current efficiency, depending on the relative concentrations in the centre and outer compartments. It is clear, that these modes of transfer are not independent of one another, and simplifying assumptions could lead to wrong conclusions especially when high ambient and interstitial concentrations occur.

However, for each set of runs there is a situation where the concentrations on both sides of the membrane are equal, and here it may be assumed that electro-osmosis is the main factor causing discrepancy between cell efficiencies and those calculated from membrane transport numbers.

From the difference in efficiencies at these points the solvent transfer in millilitres per equivalent of NaCl has been calculated, and is plotted against ambient concentration in Fig. 11. Although the results show considerable scatter it is clear that water transfer is greater at high concentrations, because of the increased solvent-ion interaction. Electro-endosmotic effects are probably secondary under these conditions because of the high solution conductivity and relatively low contribution of the charged exchange groups in the membrane pore walls.

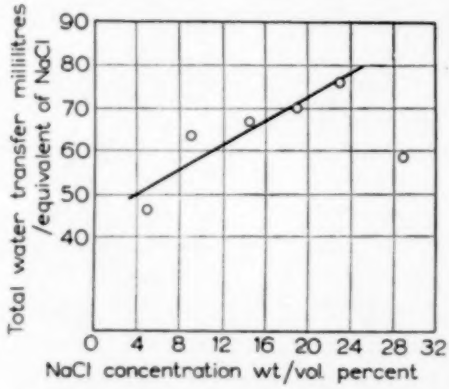

Fig. 11. Total solvent transfer in three-compartment cell, in terms of solute transfer.

If the experimental data in Figs. 8, 9 and 10 are checked using the solvent transfer data of Fig. 11 (assuming that for unequal ambient concentrations, an arithmetic mean concentration is applicable) a reasonably good agreement is obtained, showing that in a dynamic system the contribution of osmosis and diffusion is small.

4. Conclusion

It has been shown that the ion-permeable membranes " Permaplex C-10 " and " Permaplex A-10 " will operate selectively in all concentrations of sodium chloride. For a given arithmetic concentration, the membranes show greater selectivity as the concentration gradient through the membrane is increased.

A three-compartment cell has been shown to give reproducible current efficiency data for the membranes over a range of concentrations and concentration gradients.

The results of this work are being confirmed in a multi-compartment electrodialysis cell.

Acknowledgements—Grateful acknowledgement is made to Professor J. P. BAXTER for his continued interest in this research, and to R. H. BUCHANAN and P. SOUTER of the School of Chemical Engineering for helpful discussion on experimental technique.

Acknowledgement is also made to Monsanto Chemicals (Aust.) Pty. Ltd. and The Australian Atomic Energy Commission for the postgraduate scholarships which made this research possible, and to the Permutit Co. Ltd. for supply of membranes.

NOTATION

$a^{\pm}$ = Activity of solute.
E_0 = Ideal membrane potential, volts.
E = Measured membrane potential, volts.
F = The Faraday.
M = Solution concentration, molar.
M^+ = Monovalent cation.
m^+ = Monovalent cation passing anion selective membrane.
R = Gas constant, joules deg^{-1} $mole^{-1}$.
T = Absolute temperature.
t_C^+ = Transport number of cation in " Permaplex C-10. "
t_A^- = Transport number of anion in " Permaplex A-10."
t_C^- = Transport number of anion in " Permaplex C-10."
t_A^+ = Transport number of cation in " Permaplex A-10."
X^- = Monovalent anion.
x^- = Monovalent anion passing cation selective membrane.
η = Current efficiency, equivalents per Faraday.

REFERENCES

[1] ANDERSON A. M. and WYLAM C. B. *Chem. and Ind.* 1956 191.
[2] " ANON." *Chem. Eng. News* 1951 **29** 693.
[3] FRISCH N. W. *US Atomic Energy Commission* 1953 *RMO*-2322.
[4] FRISCH N. W. *US Atomic Energy Commission* 1953 *RMO*-2320.
[5] FRISCH N. W. *US Atomic Energy Commission* 1953 *RMO*-2326.
[6] *Handbook of Chemistry and Physics* 1948 The Chemical Rubber Publishing Co. Cleveland.
[7] HARNED H. S. and OWEN B. *The Physical Chemistry of Electrolytic Solutions* 1950 Reinhold N.Y.
[8] Ionics Incorporated Cambridge Mass. 1955, Bulletin No. 3.
[9] JUDA W. and MC RAE W. A. *J. Amer. Chem. Soc.* 1950 **72** 1044.
[10] JUDA W. ROSENBERG N. W., MARINSKY J. A., and KASPER A. A. *J. Amer. Chem. Soc.* 1952 **74** 3736.
[11] KRESSMAN T. R. E. *Nature* 1950 **165** 568.
[12] KUNIN R. *US Atomic Energy Commission* 1956 *RMO*-2504 Via. *Nuclear Science Abstracts* 1956 **10** 724.
[13] Permutit Co. Ltd. The, *Permutit Ion Exchange Membranes – Technical Data* 1954.
[14] SHAIR R. C., BRUINS P. F. and GREGOR H. P. *Ind. Eng. Chem.* 1956 **48** 381.
[15] SOLLNER K. J. *Electrochem. Soc.* 1950 **97** 139c.
[16] SOLLNER K. and GREGOR H. P. *J. Phys. Chem.* 1947 **51** 299.
[17] WALTERS W. R., WEISER D. W., and MAREK L. J. *Ind. Eng. Chem.* 1955 **47** 61.
[18] WIECHERS S. and VAN HOEK C. *Research* 1953 **6** 192.
[19] WILLARD H. H. and FINLEY J. J. *US Atomic Energy Commission* 1956 K-1219.
[20] WINGER A. G., BODAMER G. W. and KUNIN, R. J. *Electrochem. Soc.* 1953 **100** 178.
[21] WINGER A. G., BODAMER G. W., KUNIN R., PRIZER C. J., and HARMON G. W. *Ind. Eng. Chem.* 1955 **47** 50.

Chemical Engineering Science, 1957, Vol. 6, pp. 105 to 111. Pergamon Press Ltd.

The kinetic implications of an empirically fitted yield surface for the vapour-phase oxidation of naphthalene to phthalic anhydride

P. H. PINCHBECK*

The Coal Tar Research Association, Oxford Road, Gomersal, nr. Leeds

Abstract—A previous investigation resulted in the fitting of an empirical yield surface for phthalic anhydride formed in the vapour-phase oxidation of naphthalene. The significance of various aspects of this surface are now considered in relation to the reaction kinetics. The shape of the fitted surface is shown to exclude all but fractional order kinetics and to provide strong evidence for a particular kinetic route. Subsidiary experiments confirm an indication that a change in mechanism occurs near to 400°C. The reaction is found to be controlled by surface kinetics below this temperature.

Résumé—Des recherches antérieures ont consisté à ajuster empiriquement la surface de réaction necéssaire à la production d'anhydride phtalique par oxydation du naphtalène en phase vapeur.

L'auteur considère ici la signification des différents aspects de cette surface en rapport avec la cinétique de la réaction.

La forme de la surface exclut toute cinétique d'un ordre autre que fractionnaire et semblerait indiquer une cinétique particulière. Des expériences complémentaires confirment une variation dans le mecanisme de la réaction autour de 400°C. En-dessous de cette température, la réaction est contrôlée par la cinétique de surface.

INTRODUCTION

IN a previous paper [1] a systematic statistical study of the vapour phase oxidation of naphthalene to phthalic anhydride was carried out. For a particular $V_2O_5/K_2SO_4/SiO_2$ catalyst it was demonstrated that the phthalic anhydride yield surface was well approximated by the quadratic expression

$$\begin{aligned} Y = &- 234{\cdot}89 + 151{\cdot}61X_1 + 258{\cdot}91X_2 \\ &+ 310{\cdot}76X_3 - 19{\cdot}95X_1^2 \\ &- 60{\cdot}86X_2^2 - 73{\cdot}07X_3^2 - 50{\cdot}84X_1X_2 \\ &- 71{\cdot}46X_1X_3 - 143{\cdot}19X_2X_3 \end{aligned} \quad (1)$$

This expression was found to represent a family of hyperboloids as shown in Fig. 1. Cross sections of the surface at constant temperature are families of ellipses and Fig. 2 shows the cross section at 405°C with 70% and 80% mole conversion contours. Differentiation of equation (1) reveals the existence of a stationary point at 401°C in the form of a col or minimax (i.e. a point which represents a maximum for two variables and a minimum with respect to the third). Further calculation shows that the maxima at various temperatures increase slowly in value both above and below the minimax temperature.

Box [2] has recently drawn attention to the fact that " natural " variables, such as temperature, pressure and concentration, are used in chemical experimentation because of the convenience of measurement. The fundamental variables controlling chemical reactions (e.g. frequency of molecular collision) are usually functions of two or more of the natural variables. As a result of this, a yield surface fitted in a factor space of natural variables usually contains ridge systems. These ridge systems in the empirical surface may be related to the basic mechanism of the reaction and can be used to differentiate between various theoretically possible mechanisms [3].

IOFFE and SHERMAN [4] have studied the

*Present address : United Coke and Chemicals Co. Ltd., Sheffield.

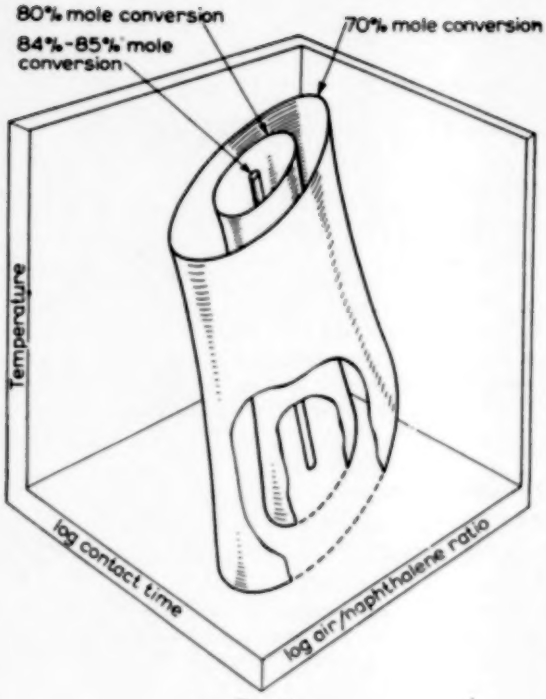

FIG. 1.

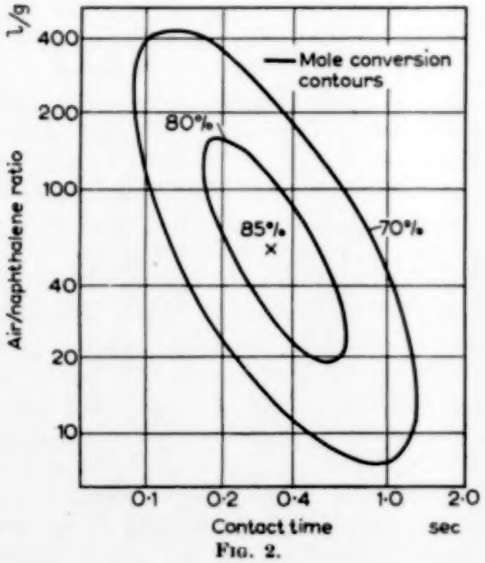

FIG. 2.

kinetics of the vapour phase oxidation of naphthalene and conclude that the reaction rate is controlled by diffusion of reactants in the catalyst pores at temperatures as low as 330°C.

The same authors [5] have also investigated the steps occurring in the oxidation reaction and have proposed the following system,

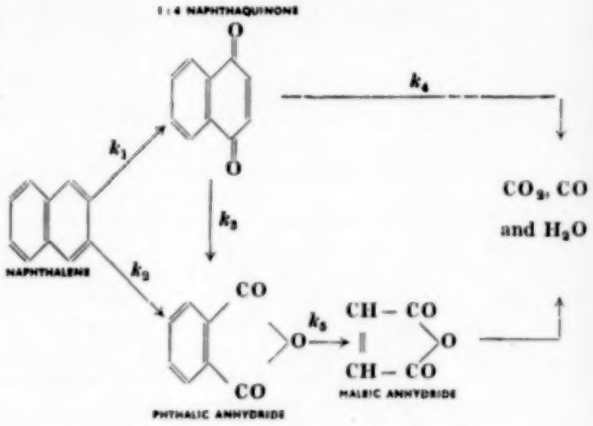

In the course of an investigation into catalysts for the oxidation of SO_2 to SO_3, TANDY [6] reported that an approximate melting point of 400°C for mixtures of V_2O_5 and K_2SO_4. The catalyst used in obtaining equation (1) contained V_2O_5 and K_2SO_4 in similar proportions to that used by TANDY.

THE FITTED YIELD SURFACE

Consideration of the form of the fitted yield surface (equation 1) reveals several significant facts;

1. The presence of a 'minimax' within the experimental region raises the possibility of a change of kinetic mechanism around this temperature.
2. The attenuated ridge systems occurring indicate a considerable degree of factor inter-dependence.
3. Although the empirical surface was fitted to experimental results spread over unusually wide regions of factor space and included mole conversions between 60 and 85% the deviations of the experimental results from the predicted results are little greater than those expected from the known experimental errors. The true yield surface is, therefore, very similar in form to the model obtained.

Table 1.

Property	40/80 *Mesh sample*	100/150 *Mesh sample*	*Remarks*
Average particle diameter cm	$2{\cdot}6 \times 10^{-2}$	$1{\cdot}25 \times 10^{-2}$	Calculated assuming perfectly spherical particles
External surface area of one average particle cm^2	$21{\cdot}1 \times 10^{-4}$	$4{\cdot}91 \times 10^{-4}$	
Average pore length cm	$0{\cdot}6 \times 10^{-2}$	$0{\cdot}3 \times 10^{-2}$	
Total surface area m^2/g B.E.T. method	38·9	38·9	Not determined separately
Percentage pore volume	34	35	
Particles per gram	$4{\cdot}42 \times 10^4$	$32{\cdot}7 \times 10^4$	
External surface area m^2/g	0·0093	0·0161	Ratio 1·73

It seemed desirable at this stage to investigate two main aspects of the yield surface : first to determine whether the reaction taking place was controlled by diffusion in the catalyst pores and whether any change in mechanism occurred near to the minimax temperature ; secondly, by adopting the kinetic system proposed by IOFFE and SHERMAN, to compare the fitted surface with surfaces generated by various theoretically derived rate equations.

REACTION RATE AND PARTICLE SIZE

If the reaction rate is retarded by diffusion of reactants in the catalyst pores then an increase in the number of pores available for reaction should give a corresponding increase in reaction rate. Accordingly a sample of microspherical V_2O_5/K_2SO_4 on silica gel catalyst, similar to that used in the previous work, was prepared. This catalyst was accurately sieved between 40 and 80 mesh screens and divided into two parts. One part was then ground down and a sample sieved out between 100 and 150 mesh. Various physical properties of these two samples were determined and are recorded in Table 1.

As the two samples are from the same original batch the number of pore mouths per unit surface area will be almost identical. Thus the number of pore mouths available in a given weight of catalyst sample is proportional to the external surface area and the finer material should contain 1·73 times as many as the coarser sample. As, however, the 100-150 mesh particles are not spherical the external surface area will be greater than that calculated and the factor is likely to be somewhat greater than 1·73.

Using identical weights of these samples, the rate of oxidation of naphthalene was examined under the same operating conditions, chosen in such a way as to obtain incomplete conversion of the naphthalene. The experimental apparatus and analytical techniques used in this work were the same as those described previously [1]. Fig. 3 shows the Arrhenius plot of first order rate constant with temperature. The energies of activation obtained from the slopes of the straight line portions were,

40/80 mesh catalyst 26·0 kcals/mole
100/150 mesh catalyst 28·0 kcals/mole

These may be compared with the results obtained by CALDERBANK [7] (26 kcals/mole), MARS and VAN KREVELEN [8] (22 kcals/mole) and IOFFE and SHERMAN [4] (27·4 kcals/mole).

It is clear that the expected increase in rate has not taken place as the constant obtained below 400°C for the finer catalyst does not exceed that from the coarser material by more

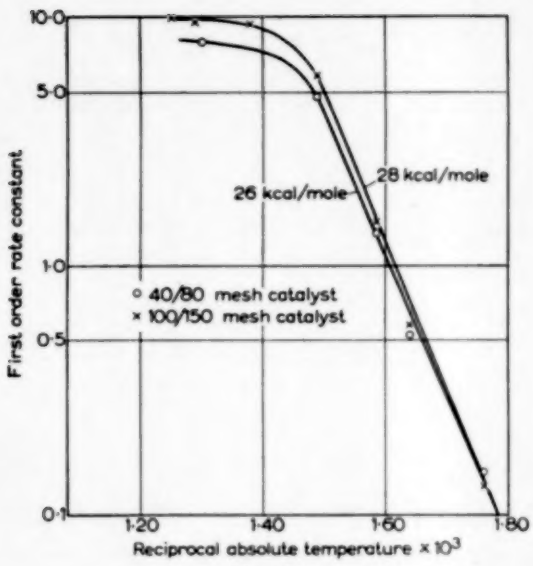

FIG. 3.

than a factor of 1·15. Also the energy of activation obtained shows that the Arrhenius relation is obeyed up to 400°C and consequently, as shown by WHEELER [4a], surface kinetics must be rate controlling up to this point. Between 400° and 500°C the difference between the two catalysts is more marked and it is possible that diffusion plays a greater part in this region. The results in the region of 500°C were the least reliable, and this point would require more careful investigation. There would seem to be no doubt, however, that the kinetic mechanism undergoes modification around 400°C as indicated by the rapid change of slope in Fig. 3. This provides support for the contention that the occurrence of a 'minimax' in the fitted surface is not a chance effect but is the result of fitting a quadratic expression to a true surface containing a major axis which has a change of slope at this point.

KINETIC ORDER AND THE YIELD SURFACE

Using as a model, the kinetic system proposed by IOFFE and SHERMAN [5] various cases may be considered and integrated rate equations deduced.

Case 1

Disappearance of naphthalene half order, subsequent steps first order.

$$C_p = \frac{C_{N_s}^{0.5}}{k_5}\left(k_2\,(1 - e^{-k_5 t}) + \frac{k_1 k_2}{k_3 + k_4}\,(1 - e^{-(k_3+k_4)t})\right) - \frac{(k_1 + k_2)\,t}{2k_5}\left(k_2 + \frac{k_1 k_3}{k_3 + k_4}\right)$$

Case 2

All steps in reaction first order.

$$C_p = \frac{k_2}{k_5 - (k_1 + k_2)}\,C_{N_s}\,(e^{-(k_1+k_2)t} - e^{-k_5 t}) + \frac{k_1 k_3}{(k_3 + k_4) - (k_1 + k_2)}\,C_{N^s}\left(\frac{e^{-(k_1+k_2)t} - e^{-k_5 t}}{k_5 - (k_1 + k_2)} + \frac{e^{-k_5 t} - e^{-(k_3+k_4)t}}{k_5 - (k_3 + k_4)}\right)$$

Case 3

Disappearance of naphthalene second order, subsequent steps first order.

$$C_p = \left(\frac{k_2}{k_5} + \frac{k_1 k_3}{k_5\,(k_3 + k_4)}\right)\left(\frac{1}{C_{N_s}^{-1} + (k_1 + k_2)\,t}\right)^2 - C_{N_s}^2\left(\frac{k_2}{k_5}\,e^{-k_5 t} + \frac{k_1 k_3}{k_5\,(k_3 + k_4)}\,e^{-(k_3+k_4)t}\right)$$

As $100\,\dfrac{C_p}{C_{N_s}}$ is equal to Y, the percentage mole conversion, these rate equations may be made equivalent to the fitted equation. The rate equations and the fitted equation then contain the same variables. Temperature appears in the rate equations by the dependence of the rate constants, initial naphthalene concentration, C_{N_s}, and air/naphthalene ratio are inversely proportional and contact time appears directly in all cases.

The rate equations may thus be compared with empirical equation on the basis of the yield surface generated in the same factor space. For convenience a two dimensional factor space at constant temperature was first considered. Using the rate constants given by IOFFE and SHERMAN, values were obtained by solution of the rate equations. The surfaces were then plotted on the same scales as those used in fitting the empirical surface. The sections so obtained are shown in Fig. 4.

It is seen that as the order of the first step increases, so the slope of the major axis (in the factor space considered) changes from negative

to positive. For this system, therefore, orders less than unity will give rise to surfaces having negative slopes and orders greater than unity will give positive slopes.

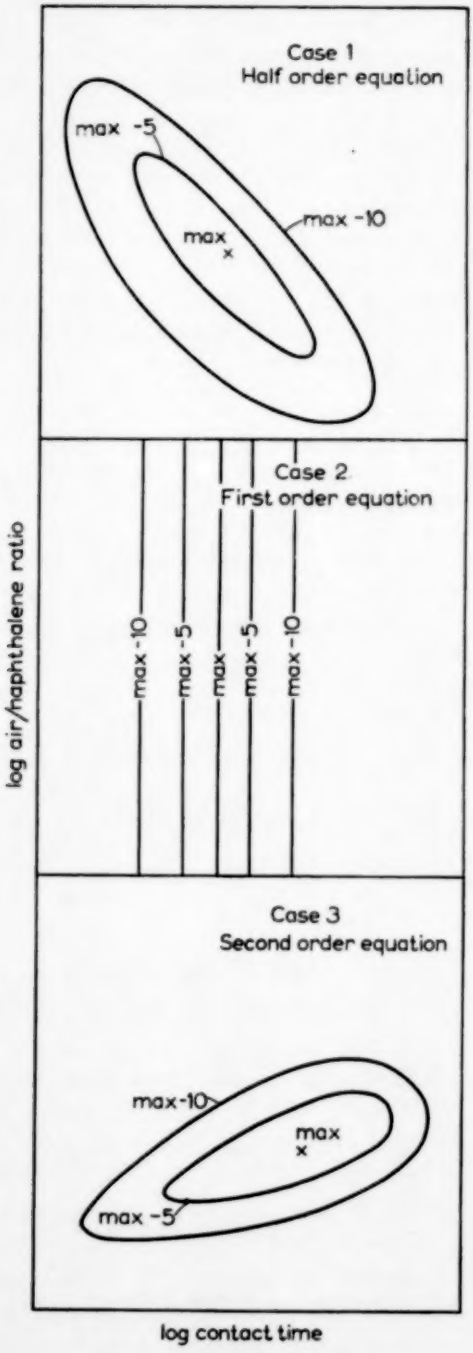

FIG. 4.

It is evident that the fractional order equation generates a yield surface of strikingly similar form to that obtained empirically and this surface was considered in greater detail. The values of the various rate constants given by IOFFE and SHERMAN do not predict maximum conversion at the same position in the factor space as the fitted equation, neither do they predict the same level of maximum. This is not surprising since the rate constants will vary in magnitude and ratio with the composition and physical form of the catalyst used. The values of the constants at any temperature will determine

(i) The maximum conversion

(ii) The position(s) in the factor space at which maximum conversion is obtained

(iii) The " spread " of the contours.

It was also found that variation of the ratios k_1/k_2 and k_3/k_4 caused variations in the slope of the major axis of the constant temperature section. Consequently, this slope is likely to vary with catalyst form and composition.

Considering the complete three dimensional factor space (i.e. including temperature) the slope of the entire surface with respect to the temperature axis will be controlled only by the rate of change of the values of the various rate constants with temperature (i.e. dependent upon the activation energy of the various steps). Within the region where surface kinetics are rate controlling this rate of change will be independent of catalyst and thus all catalysts should show a parallel major axis. In order to check this point the position of maximum conversion was determined from the fractional order equation at various temperatures and Figure 5 shows a comparison of the slopes obtained with those derived from the empirical equation. Once again a large measure of agreement exists.

CONCLUSIONS

The comparison of reaction rates obtained over different size ranges of the same catalyst indicates that, contrary to the results obtained by IOFFE

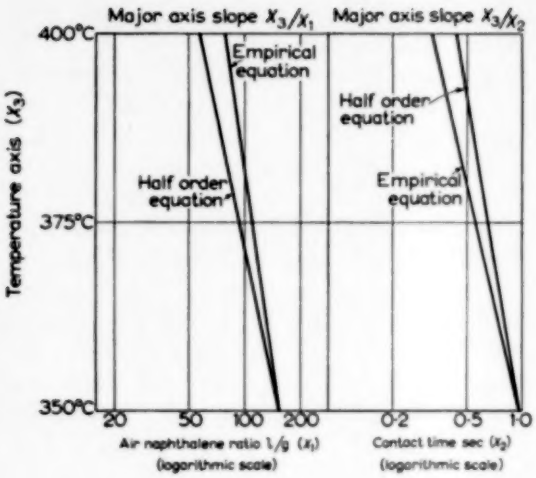

FIG. 5.

and SHERMAN [4], the reaction rate is controlled by surface kinetics up to temperature of about 400°C. In this respect the results support the views of MARS and VAN KREVELEN [8] who also employed fluidized catalysts of a similar composition. From the data of IOFFE and SHERMAN [4] it can be deduced that their catalyst was of unusually high apparent density (1·91) and consequently had a low porosity. It is also well known that variations in the treatment of silica gel can lead to widely differing pore structures. The results of IOFFE and SHERMAN may, therefore, be explained in terms of the physical form of the catalyst used.

The temperature at which the 'minimax' occurs in the fitted surface is shown to be associated with a change in kinetic mechanism, a change in state of the active catalyst components also occurs near this temperature.

From the comparison of the types of yield surface generated by various rate equations strong evidence has been obtained indicating that the vapour phase oxidation of naphthalene, under high conversion conditions, occurs with fractional order kinetics. The direction of the axes of the empirical surface would suggest an order between 0·8 and 0·9. The agreement between the empirical and theoretical surfaces provides strong support for the kinetic system proposed by IOFFE and SHERMAN [5], and the slope of the surface with respect to the temperature axis indicates that the values of activation energies deduced by these authors for the various steps are reasonable. This evidence is more powerful than the normal kinetic data in that it represents the results of some seventy experiments carried out over wide regions of factor space considered as a group.

The investigation demonstrates that the purely empirical approach, when treated systematically, can throw considerable light on the basic mechanism of the reaction under investigation and provides a new approach to complex multivariable reactions.

Acknowledgements—The author is grateful to Mr. W. D. BETTS of the Coal Tar Research Association for a discussion on the mathematics involved and to Dr. J. B. J. ZABA of I.C.I. Dyestuffs Division for his courtesy in determining the surface area of the catalyst used. He also wishes to thank the Council of the Coal Tar Research Association for permission to publish this work.

NOTATION

Y = % Mole conversion of naphthalene to phthalic anhydride

X_1 = $\log_{10}$ Air/Naphthalene Ratio litres/g

X_2 = $\log_{10}$ (Contact Time × 10) sec

X_3 = (Temperature − 330) $\frac{1}{100}$ °C

C_{N_0} = Initial concentration of naphthalene moles/litre

C_p = Final concentration of phthalic anthydride moles/litre

k_1 = Specific Rate Constant Naphthalene → 1 : 4 Naphthoquinone

k_2 = Specific Rate Constant Naphthalene → Phthalic anhydride

k_3 = Specific Rate Constant 1 : 4 Naphthoquinone → Phthalic anhydride

k_4 = Specific Rate Constant 1 : 4 Naphthoquinone → Complete combustion

k_5 = Specific Rate Constant Phthalic anhydride → Maleic Anhydride

References

[1] Franklin N. L., Pinchbeck P. H., and Popper F. *Trans. Inst. Chem. Eng.* In the press.

[2] Box G. E. P. *Biometrics* 1954 **10** 16.

[3] Box G. E. P. and Youle P. V. *Biometrics* 1955 **11** 287.

[4] Ioffe I. and Sherman Y. *J. Phys. Chem.* (*USSR*) 1954 **28** 2095.

[4a] Wheeler A. *Advances in Catalysis* 1951 **3** 250-326.

[5] Ioffe I. and Sherman Y. *J. Phys. Chem.* (*USSR*) 1955 **29** 692

[6] Tandy G. H. *J. App. Chem.* 1956 **6** Pt. 2 68.

[7] Calderbank P. H. *The Indust. Chemist* 1952 **28** 291.

[8] Mars P. and van Krevelen D. W. Proceedings of the conference on oxidation processes. *Chem. Eng. Sci.* 1954 (Special Edition).

Chemical Engineering Science, 1957, Vol. 6, pp. 112 to 115. Pergamon Press Ltd.

Fugacities in simple gas mixtures

JOHN M. PRAUSNITZ
Division of Chemical Engineering, University of California, Berkeley, California

(*Received* 6 *November* 1956)

Abstract—A method is presented for rapidly calculating the fugacity of a component in gaseous solution using only critical data for the pure components in the solution. The method is based on an extension of the theorem of corresponding states proposed by GUGGENHEIM and MCGLASHAN and is applicable to multicomponent mixtures of simple gases at moderate densities.

Résumé—L'auteur présente une méthode de calcul rapide de la fugacité d'un gaz dans un mélange de plusieurs gaz à partir des données critiques des constituants purs.

Cette méthode basée sur une généralisation du principe des états correspondants de GUGGENHEIM et MCGLASHAN peut être appliquée à des mélanges de gaz simples à densités moyennes.

FUGACITIES of components in a gaseous mixture must frequently be estimated in problems concerned with physical or chemical equilibria at advanced pressures. Since the extensive experimental data required for a rigorous solution are very seldom available it is customary to utilize approximating methods; the simplest of these is the Lewis fugacity rule which states that

$$\bar{f}_i = y_i f_i^0 \tag{1}$$

where $\bar{f}_i$ = fugacity of component i in the mixture.

f_i^0 = fugacity of pure component i at the temperature and pressure of the mixture.

y_i = mole fraction of component i in the mixture.

The Lewis fugacity rule assumes that Amagat's law of additive volumes is valid for the pressure range from zero pressure to the pressure of the mixture; this assumption is known to be invalid for many if not indeed for most cases.

More reliable methods for estimating fugacities in mixtures are the method of JOFFE [5] who utilizes Kay's pseudocritical concept, and the method of REDLICH and KWONG [7] who use for the mixture a two-parameter equation of state whose constants are a simple algebraic combination of the constants for the pure components. The method proposed in this paper does not assume Kay's rule nor the validity of any particular equation of state. Instead, it is based on an extension of the theorem of corresponding states proposed by GUGGENHEIM and MCGLASHAN [2]. This method is very easy to use and at moderate densities may be expected to give good results for simple mixtures; that is, for mixtures of nonpolar molecules whose force fields are spherically symmetric.

For a simple binary mixture the second virial coefficient B_{mix} is given by a quadratic function of the composition (6):

$$B_{mix} = B_1 y_1^2 + 2 B_{1,2} y_1 y_2 + B_2 y_2^2 \tag{2}$$

where B_1 and B_2 are the second virial coefficients of the pure components 1 and 2 respectively, and where $B_{1,2}$ is a constant for the binary mixture. GUGGENHEIM and MCGLASHAN [2] have shown that the theorem of corresponding states can be used not only to predict B_1 and B_2 but also $B_{1,2}$ provided the critical volume and critical temperature of both components are known.

The second virial coefficients for the pure components are given by

$$\frac{B_1}{V_{c_1}} = \Phi\left(\frac{T}{T_{c_1}}\right) \quad \text{and} \quad \frac{B_2}{V_{c_2}} = \Phi\,\frac{T}{T_{c_2}} \tag{3}$$

where T = temperature; V = volume per mole; and subscript c denotes critical.

The data for numerous simple gases show that the function Φ is a universal function which is very nearly the same for all simple gases.

GUGGENHEIM and MCGLASHAN have examined the data for various simple binary mixtures and have shown that the coefficient $B_{1,2}$ can be represented by

$$\frac{B_{1,2}}{V_{c_{1,2}}} = \Phi\left(\frac{T}{T_{c_{1,2}}}\right) \tag{4}$$

where the function Φ is the same as that for the pure components. The terms $V_{c_{1,2}}$ and $T_{c_{1,2}}$ are found from the corresponding terms for the pure components by means of the common mixing rules as recommended by HIRSCHFELDER *et al.*, in their work on transport properties [4] :

$$V_{c_{1,2}}{}^{1/3} = \tfrac{1}{2}\left[V_{c_1}{}^{1/3} + V_{c_2}{}^{1/3}\right] \tag{5}$$

$$T_{c_{1,2}} = \sqrt{T_{c_1} T_{c_2}} \tag{6}$$

In most problems it is more convenient to use the compressibility factor rather than virial coefficients. The relationship between the compressibility factor z and the virial coefficient B is given by

$$z = \frac{PV}{RT} = 1 + \frac{BP}{RT} + \ldots\ldots \tag{7}$$

If higher terms in the virial expansion are neglected, then at constant pressure and temperature z is a linear function of B and from equation (2) the relationship between z_{mix}, the compressibility factor for the mixture, and the composition is given by

$$z_{mix} = y_1{}^2 z_1 + 2y_1 y_2 z_{1,2} + y_2{}^2 z_2 \tag{8}$$

where z_1 and z_2 are the compressibility factors for pure components 1 and 2 respectively, at the temperature and pressure of the mixture. (If it is assumed that $z_{1,2} = \frac{1}{2}(z_1 + z_2)$ then equation (8) reduces to Amagat's law of additive volumes.)

The compressibility factors for the pure components are readily found from the generalized compressibility charts if the critical pressures and temperaturse of the pure components are available. To find the compressibility factor $z_{1,2}$ it is necessary to define a critical pressure $P_{c_{1,2}}$ which can be found by extending the previously mentioned mixing rules as follows :

The critical pressure P_c for a pure component is given by

$$P_c = \frac{z_c RT_c}{V_c} \tag{9}$$

where z_c = compressibility factor at the critical point. For $P_{c_{1,2}}$ we therefore write

$$P_{c_{1,2}} = \frac{z_{c_{1,2}} RT_{c_{1,2}}}{V_{c_{1,2}}} \tag{10}$$

where $V_{c_{1,2}}$ and $T_{c_{1,2}}$ are given by equations (5) and (6). The term $z_{c_{1,2}}$ is some average between z_{c_1} and z_{c_2} ; fortunately z_c does not vary much for simple molecules and therefore any method for averaging will give very nearly the same result as any other method. It is simplest to adopt the arithmetic average and equation (10) then becomes

$$P_{c_{1,2}} = \frac{4\,(z_{c_1} + z_{c_2})\,R\sqrt{T_{c_1} T_{c_2}}}{\left[V_{c_1}{}^{1/3} + V_{c_2}{}^{1/3}\right]^3} \tag{11}$$

The fugacity of a component in a binary mixture can readily be calculated from equation (8) and can be expressed in the form

$$\bar{f}_1 = \gamma_1 f_1{}^0 y_1 \tag{12}$$

where γ_1 = activity coefficient of component 1 in the mixture.

$f_1{}^0$ = fugacity of pure component 1 at the same temperature and pressure as those of the mixture.

The ratio of the fugacity of a component in a binary mixture to its partial pressure is given by an equation previously derived by JOFFE [5] :

$$\ln \frac{\bar{f}_1}{y_1 P} = \ln (f/P)_{mix} - y_2 \left(\frac{\partial \ln (f/P)_{mix}}{\partial y_2}\right)_{T,P} \tag{13}$$

The ratio of the fugacity of a pure gas to the total pressure is related to the compressibility factor of that gas by

$$\ln (f^0/P)_1 = -\int_0^P \left(\frac{1 - z_1}{P}\right) dP \tag{14}$$

and similarly for the mixture as a whole

$$\ln (f/P)_{mix} = -\int_0^P \left(\frac{1 - z_{mix}}{P}\right) dP \tag{15}$$

Substituting equation (15) into equation (13), inverting the order of integration and differentiation, and then substituting equations (8), (14), and (12) yields a simple result for the activity coefficient γ:

$$\ln \gamma_1 = K y_2^2 \tag{16}$$

where

$$K = 2 \ln (f/P)_{1,2} - \ln (f^\circ/P)_1 - \ln (f^\circ/P)_2 \tag{17}$$

Similarly

$$\bar{f}_2 = \gamma_2 y_2 f_2^0 \tag{18}$$

and

$$\ln \gamma_2 = K y_1^2 \tag{19}$$

The constant K in equation (19) is the same as that in equation (16).

The three terms which comprise K can readily be found from the generalized fugacity coefficient charts which express f/P as a function of reduced pressure and reduced temperature. The critical constants to be used in the evaluation of the first term are given by equations (11) and (6).

If Amagat's law holds for the entire pressure range from zero pressure up to the pressure of interest, then $K = 0$, and $\gamma_1 = \gamma_2 = 1$.

APPLICABILITY

In the derivation given above all virial coefficients higher than the second were neglected; the proposed method of calculation therefore is only valid for moderate densities. Equation (8) predicts that the volume change in mixing is a symmetric parabolic function of the composition which is in agreement with experimental results for simple mixtures at moderate densities. The data for the nitrogen-ethylene system at 50°C (3), for example, show that this symmetric parabolic relationship holds quite well for pressures up to about 100 atmospheres. Accoridng to Amagat's law, of course, the volume change on mixing is zero.

Some results for the nitrogen-ethylene system are shown in Table 1. The activity coefficients predicted from equation (16) and the generalized charts are compared with those calculated by BENNETT [1] from the data of HAGENBACH and COMINGS [3]. The agreement is good.

Table 1. *Activity Coefficients for Nitrogen-Ethylene Mixtures at 50°C*

Pressure (atm)	*Mol Fraction Nitrogen*	γ_{N_2}		$\gamma_{C_2H_4}$	
		Calc.	*Ref.* [1]	*Calc.*	*Ref.* [1]
50	0·0	1·18	1·19	1·00	1·00
	0·2	1·10	1·12	1·01	1·01
	0·4	1·06	1·06	1·02	1·02
	0·6	1·02	1·02	1·06	1·07
	0·8	1·01	1·01	1·10	1·11
	1·0	1·00	1·00	1·18	1·18
100	0·0	1·41	1·45	1·00	1·00
	0·2	1·25	1·27	1·01	1·01
	0·4	1·11	1·14	1·06	1·06
	0·6	1·06	1·06	1·11	1·14
	0·8	1·01	1·01	1·25	1·27
	1·0	1·00	1·00	1·41	1·45

The approximate range of temperature and pressure for which this method is applicable is that for which virial coefficients higher than the second can be neglected without serious error; this range is for densities up to about one-half of the critical. As a rough rule, therefore, the method is applicable for the range where

$$\frac{V}{V_c} > 2$$

Substituting $V = zRT/P$ and using a value of 0·29 for the compressibility factor at the critical point the valid range is approximately given by

$$\frac{zT_R}{P_R} > 0{\cdot}58$$

where the critical properties of the mixture may be estimated by Kay's rule.

EXTENSION TO MULTICOMPONENT MIXTURES

The above derived method for a binary mixture can readily be extended to a multicomponent system by the well-known methods summarized by WOHL [8]. Since equations (16) and (19) for the binary case are the result of a two-suffix expansion for the excess free energy, extension

to a multicomponent system requires only constants for all the binaries in the multicomponent mixture. The activity coefficient for a species r in a mixture of n components if given by

$$\ln \gamma_r = \sum_{i=1}^{n} y_i K_{ir} - \tfrac{1}{2} \sum_{i=1}^{n} \sum_{j=1}^{n} y_i y_j K_{ij} \qquad (20)$$

The coefficients K_{ij} are evaluated from the generalized fugacity chart as indicated previously; that is,

$$K_{ij} = 2 \ln (f/P)_{ij} - \ln (f^\circ/P)_i - \ln (f^\circ/P)_j$$

When $i = j$ the coefficient K vanishes as expected.

Nomenclature

B = second virial coefficient
$\bar{f}_i$ = fugacity of component i in the mixture
f_i^0 = fugacity of pure component i at the temperature and pressure of the mixture
K = defined by equation (17)
P = pressure
R = gas constant
T = temperature
V = volume
y = mol fraction
z = compressibility factor
γ = activity coefficient
Subscript c denotes critical
Subscript R denotes reduced

References

[1] Bennett C. O. *Chem. Eng. Prog. Symposium Series No.* 7 1953 **46.**

[2] Guggenheim E. A. and McGlashan M. L. *Proc. Roy. Soc.* 1951 **A206** 448.

[3] Hagenbach W. P. and Comings E. W. *Ind. Eng. Chem.* 1953 **45** 606.

[4] Hirschfelder J. O., Curtiss C. F., and Bird R. B. *Molecular Theory of Gases and Liquids*, New York, John Wiley and Sons (1954).

[5] Joffe J. *Ind. Eng. Chem.* 1948 **40** 1738.

[6] Lennard-Jones J. E. and Cook W. R. *Proc. Roy. Soc.* 1927 **A115** 334.

[7] Redlich O. and Kwong J. *Chem, Rev.* 1949 **44** 233.

[8] Wohl K. *Trans. Amer. Inst. Chem. Engrs.* 1946 **42** 215.

Chemical Engineering Science, 1957, Vol. 6, pp. 116 to 122. Pergamon Press Ltd.

Prediction of ternary liquid-liquid equilibrium from binary data

(for the system furfural—iso-octane—benzene)

J. W. KENNY

Chemical Engineering Department, University of Sydney

(*Received* 28 *September* 1956)

Abstract—The distribution of benzene in the ternary system furfural – iso-octane – benzene was predicted from binary data, obtained by total pressure measurements on the systems benzene – iso-octane, benzene – furfural and iso-octane – furfural. The distribution was predicted using the two – suffix equations of VAN LAAR [2] and the semiempirical methods of HILDEBRAND [5] and SCHEIBEL and FRIEDLAND [6].

The system carbon tetrachloride – acetic acid was also investigated by the total pressure method.

The binary data obtained from these total vapour pressure measurements can be taken as fairly reliable, since azeotropes were picked up quite accurately and REDLICH and KISTER plots showed that the results were thermodynamically consistent. The method of calculation ensures that the final activity coefficients are a very good representation of the original pressure measurements.

This binary data, when applied in the VAN LAAR equations for the prediction of ternary equilibrium, gives a distribution which is consistently 1-2 mole % of solute low in the iso-octane-rich phase when compared with HENTY's experimental distribution. The distribution predicted by HILDEBRAND's method is more accurate than the VAN LAAR prediction in the region near the plait point, but is fallacious in the near binary regions in that it indicates a molar solutrope.

The ternary VAN LAAR distribution obtained using the binary data and the binodal curve is accurate in the region near the plait point, but remains 1-2 mole % of solute in error near the binaries.

SCHEIBEL and FRIEDLAND's correlation is generally more satisfactory than VAN LAAR's except near the binaries, where it indicates a molar solutrope, which does not in fact exist.

Résumé—L'auteur étudie la distribution du benzène dans le système ternaire furfural–isooctane–benzène en fonction des pressions totales des systèmes binaires : benzène–isooctane, benzène–furfural, isooctane–furfural. Il étudie cette distribution en utilisant les équations de VAN LAAR et les méthodes semi-empiriques de HILDEBRAND et de SCHEIBEL et FRIEDLAND.

Le système tétrachlorure de carbone–acid acétique a été également étudié parla mesure des pressions totales.

On peut admettre que les données binaires obtenues à partir des mesures de pression sont à peu près exactes, étant donné que les azéotropes sont retrouvés avec exactitude et que les courbes de REDLICH et KISTER donnent des résultats compatibles thermodynamiquement. La méthode de calcul garantit que les coefficients d'activité sont en accord avec les pressions initiales.

L'auteur applique ces données binaires à l'équation de VAN LAAR en vue d'obtenir l'équilibre ternaire : il en résulte une distribution inférieure de 1 à 2 mole % de soluté dans la phase riche en isooctane comparée à la distribution expérimentale de HENTY. La distribution prévue par la méthode de HILDEBRAND est plus précise que celle de VAN LAAR dans la région du point de courbure, mais ne convient pas dans les régions binaires en ce sens qu'elle indiquerait un solutrope molaire.

La distribution de VAN LAAR basée sur cette méthode, données binaires et courbes binodales, est satisfaisante dans le voisinage du point de courbure, mais accuse une erreur de 1 à 2 mole % de soluté près des zones binaires.

La relation de SCHEIBEL et FRIEDLAND est en général plus satisfaisante que celle de VAN LAAR sauf dans les régions binaires où elle semblerait indiquer un solutrope molaire qui, en fait, n'existe pas.

Introduction

The aim of the work was to investigate the accuracy with which certain ternary liquid-liquid equilibrium relationships could be predicted from binary data and some ternary data. Various mathematical procedures have been proposed by Wohl [1], van Laar [2], Benedict [3], Redlich and Kister [4] and others. In addition to these, empirical or semiempirical methods have been suggested by Hildebrand [5] and Scheibel and Friedland [6]. These methods must be reliable since it is essential that the distribution of one liquid between the other two solvents be known accurately before the process can be applied to industry.

Binary data were obtained by the measurement of total vapour pressures on a range of binary liquid mixtures. From these readings the activity coefficient-composition curves were calculated by the method due to Barker [7].

The ternary distribution was predicted by combining the data for the three relevant binaries. Experimental ternary data were supplied by C. J. Henty who is studying at Sydney a quaternary system with iso-octane – furfural – benzene as one ternary.

Apparatus and Materials

A sketch of the total pressure apparatus is shown in Fig. 1. The vapour space was warmed by an isotape to prevent distillation and consequent alteration in liquid mixture composition. Provision was made for agitation under vacuum by means of a nickel paddle actuated by the rotating magnet of a magnetic stirrer.

A Cenco-Megavac pump was used to obtain a vacuum of the order of 0·1 microns of mercury. Water at 25·0°C for the bath in which the phial was immersed was circulated from a large laboratory tank by means of a centrifugal pump. Pressure differentials could be read to 0·01 mm of mercury with a cathetometer. Liquid nitrogen in vacuum flasks was used in the vapour traps and for freezing purposes.

Components of a very high degree of purity were supplied by R. G. H. Prince and C. J. Henty, who were engaged on liquid-liquid equilibrium researches in the Chemical Engineering Department of the University of Sydney. Important physical constants for these components are listed in Table 1.

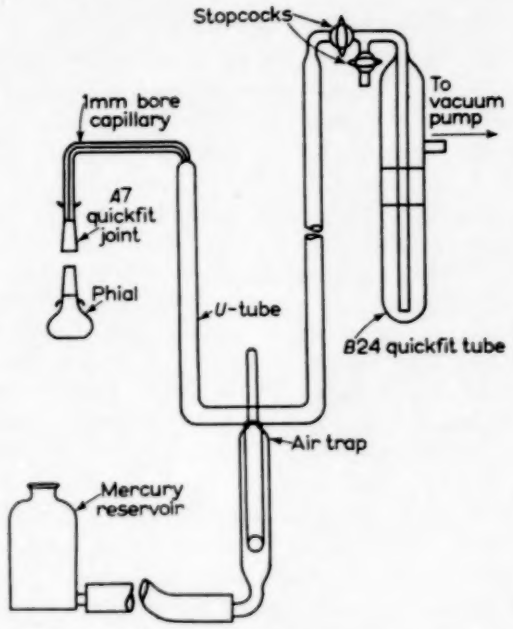

Fig. 1. Sketch of Total Pressure Apparatus.

Table 1

Properties	*Benzene*	*Isooctane*	*Furfural*	*Carbon tet.*	*Acetic acid*
Boiling point	80·1°C		161·7°C	76·7°C	117·9°C
Density, 25°C	0·8736 g/ml	0·68789 g/ml	1·15482 g/ml	1·5846 g/ml	1·0438 g/ml
Refractive index, n_D^{25}		1·38896			
Freezing point	5·47°C		− 38·8°C		16·55°C

These components were stored in sealed Winchesters and were carefully dispensed from automatic burettes fitted with drying tubes. In this way the liquids retained their high degree of purity throughout the experiments.

EXPERIMENTAL PROCEDURE

The binary mixtures were calculated roughly in terms of the volumes of the pure components. These volumes were introduced into a stoppered 50 ml conical flask which was weighed accurately after each addition of liquid.

The vapour pressure was determined in the following fashion :— the phial was almost filled with the liquid mixture, which was then stirred gently to remove air bubbles and frozen. The apparatus was evacuated, the mercury raised into the U-tube and zero levels read. The mixture was then thawed, stirred, and allowed to come to equilibrium at 25·0°C, when final levels were read. The change in mercury levels in the U-tube was the apparent vapour pressure of the mixture in the phial. Actually this figure had to be corrected for the presence of occluded air and other permanent gases. These can only be removed by vacuum sublimation and this alters the liquid mixture composition, a feature which was undesirable in this work.

Table 2. *System Carbon Tetrachloride – Acetic Acid*

Run no.	*Mole fraction carbon tetrachloride*	*Mole fraction acetic acid*	*Total vapour pressure mm Hg*
1	0·0000	1·0000	15·2
2	0·0209	0·9791	30·0
3	0·0386	0·9614	33·0
4	0·2987	0·7013	87·0
5	0·5030	0·4970	99·2
6	0·7000	0·3000	110·0
7	0·9180	0·0820	121·0
8	0·9640	0·0360	124·0
9	0·9780	0·0220	118·8
10	1·0000	0·0000	111·0

The apparent vapour pressures of the pure components were in error by from about 1 mm of mercury for those with low vapour pressures to about 4 mm of mercury for those with high vapour pressures. Intermediate mixtures were corrected proportionately to their compositions. These corrections were also checked by altering the vapour volume slightly and noting the change in total pressure. Knowing the initial and final volumes from the dimensions of the apparatus, the pressure of permanent gases causing such pressure change was then calculated, from Boyle's Law. This pressure for one particular vapour volume was then subtracted from the total pressure at that volume, giving the mixture vapour pressure.

EXPERIMENTAL READINGS

The literature [8] gives the minimum boiling azcotrope at 0·927 mole fraction carbon tetrachloride.

Table 3. *System Benzene – Iso-octane*

Run no.	*Mole fraction benzene* x_C	*Mole fraction iso-octane* x_A	*Total vapour pressure mm Hg*
1	0·0000	1·0000	49·0
2	0·0520	0·9480	59·8
3	0·1036	0·8964	66·0
4	0·2980	0·7020	80·9
5	0·4950	0·5050	88·9
6	0·6930	0·3070	94·8
7	0·9000	0·1000	98·7
8	0·9468	0·0532	99·2
9	1·0000	0·0000	95·2

The literature [8] gives the azeotrope as 0·981 mole fraction benzene.

Table 4. *System Benzene – Furfural*

Run no.	*Mole fraction benzene* x_C	*Mole fraction furfural* x_B	*Total vapour pressure mm Hg*
1	0·0000	1·0000	1·6
2	0·0521	0·9479	12·0
3	0·1027	0·8973	21·0
4	0·3045	0·6955	47·4
5	0·5060	0·4940	64·6
6	0·7035	0·2965	78·0
7	0·8997	0·1003	90·2
8	0·9526	0·0474	92·7
9	1·0000	0·0000	95·2

Table 5. System Iso-octane – Furfural

Run no.	*Mole fraction iso-octane* x_A	*Mole fraction furfural* x_B	*Total vapour pressure* mm Hg
1	0·0000	1·0000	1·6
2	0·0170	0·9830	26·0
3	0·0450	0·9550	52·2
4	0·9550	0·0450	54·0
5	0·9790	0·0210	52·0
6	1·0000	0·0000	49·0

The terminal solubilities as determined by Mr. HENTY are :

(1) { 0·0431 mole fraction iso-octane
0·9569 mole fraction furfural

(2) { 0·9461 mole fraction iso-octane
0·0539 mole fraction furfural

Total pressure measurements were also made on six ternary equilibrium mixtures. The experimental readings are presented in Table 6, where they are compared with the pressures calculated from the formula

$$P = P_1 \gamma_1 x_1 + P_2 \gamma_2 x_2 + P_3 \gamma_3 x_3$$

where the activity coefficients are calculated by the VAN LAAR equations.

EXPERIMENTAL RESULTS

Complete activity coefficient-composition relationships for three of the four binaries studied are given by Figs. 2-4, inclusive. The extrapolated end values, which are the constants used in the VAN LAAR equations etc., are marked. It should be noted that these have to be divided by 2·303 to reduce them to the common logarithm basis on which the equations are worked.

For the almost immiscible system iso-octane–furfural these end values were calculated from mutual solubility data.

The two-suffix VAN LAAR equations for the activity coefficients in the ternary reduced to :

$$\log \gamma_A = \frac{1{\cdot}303\, x_B^2 + 0{\cdot}534\, x_C^2 + 1{\cdot}552\, x_B x_C}{(x_A + 0{\cdot}936\, x_B + 1{\cdot}041\, x_C)^2}$$

$$\log \gamma_B = \frac{0{\cdot}270\, x_C^2 + 1{\cdot}583\, x_A^2 + 1{\cdot}096\, x_A x_C}{(x_B + 0{\cdot}678\, x_C + 1{\cdot}068\, x_A)^2}$$

$$\log \gamma_C = \frac{0{\cdot}474\, x_A^2 + 0{\cdot}871\, x_B^2 - 0{\cdot}040\, x_A x_B}{(x_C + 0{\cdot}961\, x_A + 1{\cdot}476\, x_B)^2}$$

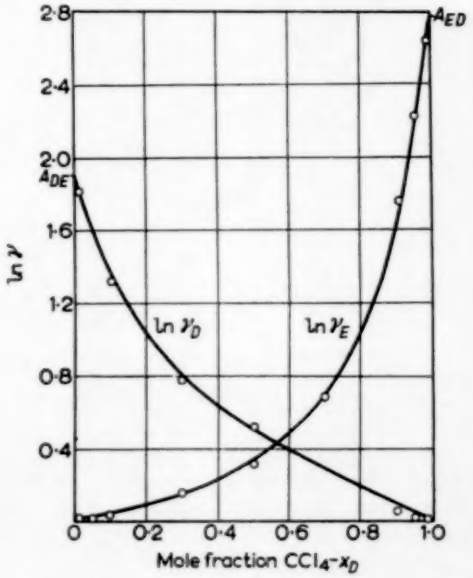

FIG. 2. Plot ln γ vs. x for carbon tetrachloride – acetic acid.

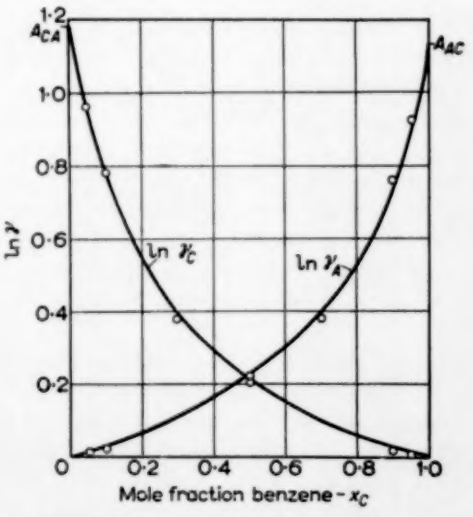

FIG. 3. Plot ln γ vs. x for benzene – iso-octane.

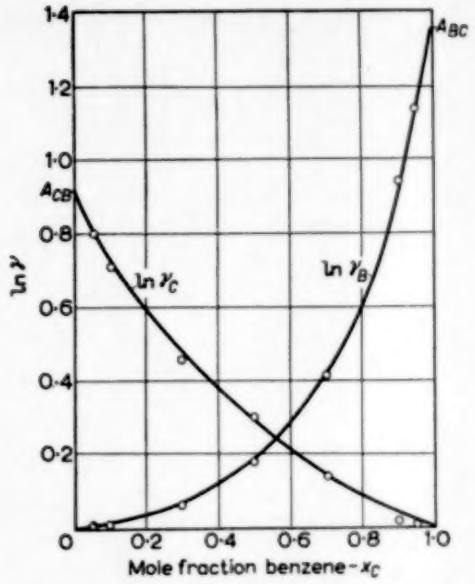

FIG. 4. Plot ln γ vs. x for benzene – furfural.

Figures 5-8, inclusive, present a comparison of ternary equilibrium data predicted by various mathematical and empirical methods with HENTY's experimental data.

DISCUSSION OF EXPERIMENTAL RESULTS

(A) *Binary Data*

The theory underlying the method of calculation of the binary activity coefficient-composition curves is such that the final results are a very good representation of the original total pressure measurements. The constants obtained by extrapolating the curves were checked by applying the VAN LAAR equation to the experimental points nearest $x_1 = 0$ and $x_1 = 1{\cdot}0$ and the agreement between extrapolated and calculated constants was always within 1% of error.

These constants should be quite reliable, since such azeotropes as existed were picked up quite accurately and REDLICH and KISTER plots for the three miscible binaries gave nett areas under the curves = zero with an error of less than 1%, proving the data to be thermodynamically consistent.

(B) *Prediction of Ternary Data*

(*a*) *From binary data only*

Figs. 5 and 6 show the degree of agreement between experiment and prediction using binary data alone. From Fig. 5 it can be seen that

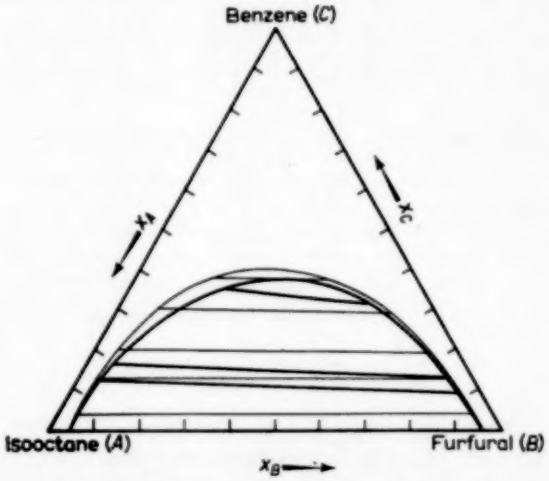

FIG. 5. Prediction vs. Experiment for system iso-octane – furfural –benzene (triangular).

Key

——— Predicted VAN LAAR results – upper curve.

——— HENTY's experimental data.

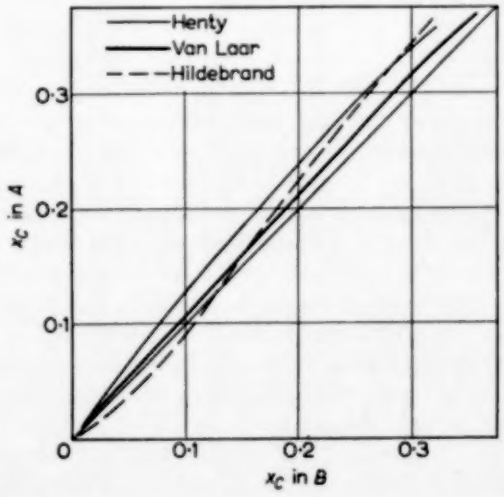

FIG. 6. Prediction vs. Experiment for molar distribution in system iso-octane – furfural – benzene from binary data only.

the two-suffix VAN LAAR equations predict the binodal curve quite accurately in the region near the binaries, but fall down near the plait point. The prediction of the tie lines is far from accurate and Fig. 6 shows that the predicted distribution is consistently 1-2 mole % of benzene too low in the iso-octane rich phase.

The tie lines resulting from VAN LAAR predictions are almost horizontal in the lower region of the triangular diagram and as the percentage of solute increases the slope of the tie lines towards the furfural apex increases. At no stage is the slope as great as that of HENTY's experimental tie lines and the discrepancy between tie line extremities is sometimes as much as 4 mole % of benzene.

The VAN LAAR distribution giving almost horizontal tie lines comes very close to predicting a molar solutrope, while the HILDEBRAND correlation does in fact predict one at 13 mole % benzene in each phase. No such solutrope exists in the system and although the HILDEBRAND method correlates well near the plait point, it can in general be said that these binary predictions are not sufficiently acucrate for application to the design of industrial extraction equipment.

(*b*) *From binary data and some ternary data*

Figs. 7 and 8 show the improvement in the accuracy of prediction gained by using HENTY's experimental binodal curve in conjunction with the binary constants obtained from total pressure measurements.

The VAN LAAR prediction is still consistently 1-2 mole % of solute in error in the lower portions of the diagram, but near the plait point, i.e. at about 30 mole % benzene, this error falls to 0·5 mole % of solute. From a theoretical viewpoint this improvement is pleasing, but from a practical point of view it is of little importance, since it is generally the lower section of the ternary diagram which is used in the design of extraction processes.

The SCHEIBEL and FRIEDLAND correlation, like that of HILDEBRAND, predicts a molar solutrope at about 10 mole % benzene and is in error by as much as 3 mole % of benzene in either phase at concentrations lower than 10 mole % benzene.

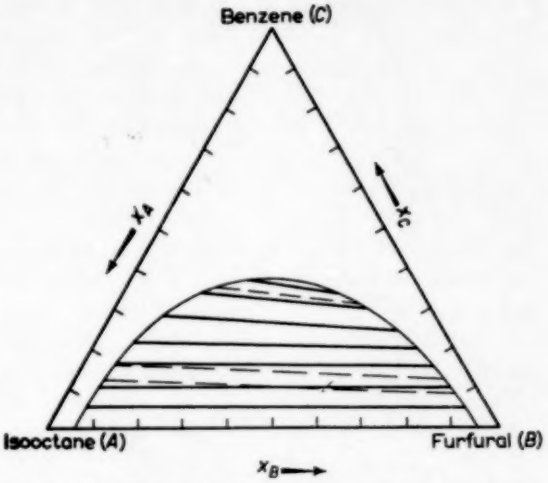

FIG. 7. Equilibrium tie lines for the system iso-octane – furfural – benzene (triangular).

Key

——— Predicted from binary data given ternary saturation curve.

– – – HENTY's experimental tie lines

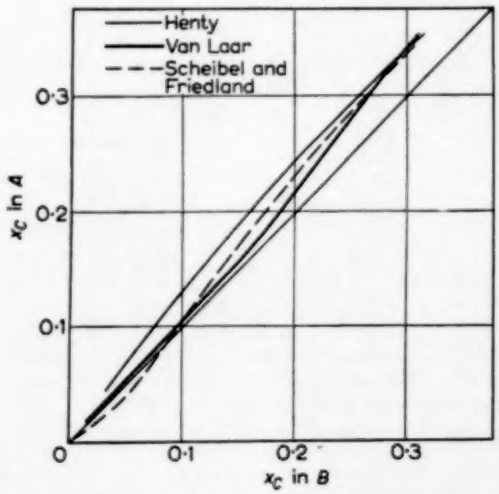

FIG. 8. Prediction v. Experiment for molar distribution is system iso-octane – furfural – benzene – given binodal curve.

Above this, however, the SCHEIBEL and FRIEDLAND prediction is by far the most satisfactory and is consistently less than 1 mole % benzene in error. Once again, however, it must be admitted that this prediction is unsatisfactory for industrial application because of the high errors in the

near-binary regions of the ternary distribution diagram.

The improvement in ternary prediction resulting from the use of the three-suffix MARGULES equations (which contain a ternary constant in addition to the original binary constants) were cursorily investigated. As far as could be judged from the few calculations made, the effect of introducing the ternary constant was to bring the predicted distribution into very much closer agreement with the experimental results. The most convenient method of estimating the ternary constant appears to be from a knowledge of one equilibrium tie line. The constant C can be solved for directly by equating the activities of the solute (expressed in terms of mole fractions, binary constants and the ternary constant C) at the two extremities of the tie line.

The calculations entailed in fully applying the three-suffix ternary MARGULES equations are very tedious but it is felt that the increased accuracy of prediction would justify the extra work.

(C) *Measurements on Ternary Equilibrium Mix ures*

Table 6

Mole fraction iso-octane- x_A	*Mole fraction furfural* x_B	*Mole fraction benzene* x_C	*Pressure as measured mm Hg*	*Pressure as calculated mm Hg*
0·0798	0·7972	0·1230	69·2	69·5
0·0588	0·8995	0·0418	57·1	57·3
0·1285	0·6450	0·2265	77·1	79·5
0·8931	0·0545	0·0525	60·4	60·3
0·8077	0·0720	0·1203	72·0	71·6
0·6042	0·1439	0·2519	81·3	81·0

Table 6 illustrates the excellent agreement between experimental and predicted total pressures for ternary equilibrium mixtures. The error in most cases is less than 1%.

Predicted figures came from applying the formula

$$P = P_1 \gamma_1 x_1 + P_2 \gamma_2 x_2 + P_3 \gamma_3 x_3$$

where the activity coefficients are calculated by the VAN LAAR equations.

Acknowledgements—The writer is indebted to R. G. H. PRINCE, who directed the work and supplied some of the pure liquids; and particularly to C. J. HENTY who supplied the rest of the pure components, made up the ternary equilibrium mixtures used and determined the experimental ternary equilibrium data reported herein; and to W. J. MCMANAMEY, whose comments and suggestions were of considerable benefit to the author in compiling this paper.

NOMENCLATURE

A = constant in MARGULES, VAN LAAR, equations
= limit of log γ as $x \to 0$
= component of a solution
a = activity
B = component of a solution
C = constant in 3-suffix ternary MARGULES equations
= component of a solution
P = total vapour pressure, mm mercury
P_1 = vapour pressure of component 1, mm mercury
x = mole fraction in a liquid
γ = activity coefficient

Subscripts

A = component A — iso-octane
B = ,, B — furfural
C = ,, C — benzene
D = ,, D — carbon tetrachloride
E = ,, E — acetic acid
AB = component A in a B-rich solution, etc.

REFERENCES

[1] WOHL KURT *Trans. Amer. Inst. Chem. Engrs.* 1946 **42** 215.
[2] VAN LAAR J. J. Z. *Phys. Chem.* 1910 **72** 723.
[3] BENEDICT M., JOHNSON C. A., SOLOMON E., and RUBEN L. C. *Trans. Amer. Inst. Chem. Engrs.* 1945 **41** 371.
[4] REDLICH OTTO and KISTER A. J. *Ind. Eng. Chem.* 1948 **40** 345.
[5] HILDEBRAND J. H. *Solubility of Non-Electrolytes* 1936 Reinhold.
[6] SCHEIBEL E. G. and FRIEDLAND D. *Ind. Eng. Chem.* 1947 **39** 1329.
[7] BARKER J. A. *Austral. J. Chem.* 1953 **6** 207.
[8] HORSLEY L. H. *Ind. Eng. Chem. Analyt.* 1947 **19** 508.

Chemical Engineering Science, 1957, Vol. 6, pp. 123 to 131. Pergamon Press Ltd.

The equations of change and the macroscopic mass, momentum, and energy balances

R. Byron Bird

Department of Chemical Engineering, University of Wisconsin, Madison, Wisconsin

(*Accepted for publication in revised form 6 September 1956*)

Abstract—It is well-known how the Bernoulli equation of mathematical hydrodynamics is obtained by forming the scalar product of the velocity vector with the *Euler* equation of motion for an *inviscid* fluid and integrating the resulting equation along a *streamline* (Streeter [8]). It is here shown how the "engineering Bernoulli equation" – containing the mechanical work term and the friction loss term – may be obtained by a similar integration of the *Navier-Stokes* equation of motion for a *viscous* fluid over the *volume* of a flow system. For the sake of completeness it is first shown how the macroscopic mass, momentum, and energy balances used in engineering are obtained from the "equations of change" of theoretical physics. In these derivations the role played by the moving surfaces is taken into account explicitly, and the fluid flowing in the system may consist of several chemical species with chemical reaction occurring. The development leads to the unsteady state expressions for the macroscopic balances and the Bernoulli equation. The correct types of average velocities to be used in the macroscopic balances arise naturally in the course of the derivations.

Résumé—L'obtention de l'équation de Bernoulli en mécanique des fluides est bien connue à partir du produit scalaire du vecteur vitesse par l'équation d'Euler du mouvement d'un fluide non visqueux que l'on intègre le long d'une ligne de courant (Streeter 8). L'auteur indique ici comment on peut obtenir par une intégration analogue de l'équation de Navier-Stokes, équation de mouvement d'un fluide visqueux, l'équation de Bernouilli utilisable pratiquement, contenant les termes de travail mécanique et de perte de charge par frottement. Dans un souci de précision l'auteur montre comment il obtient à partir des équations d'échange de la physique théorique, les bilans massiques, les bilans des moments et les bilans énergétiques. Il tient compte aussi dans ses calculs ; de façon explicite, du rôle joué par les surfaces en mouvement, et du fait que le fluide qui s'écoule peut contenir plusieurs espèces chimiques en réaction. Le développement conduit à des expressions d'états de transition pour les bilans macroscopiques et l'équation de Bernouilli.

Les expressions correctes des vitesses moyennes dont on se sert dans les bilans macroscopiques apparaissent naturellement en cours de calculs.

The Equations of Change for a Multicomponent Single-Phase Fluid

The differential equations describing the motion of a fluid containing ν chemical species are the "equations of change" which may be derived from non-equilibrium statistical mechanics (Hirschfelder *et al.* [3]). These equations in the forms given here are applicable to both laminar and turbulent flow, and apply to non-Newtonian as well as Newtonian fluids. They may be written in two equivalent forms : In the *first* form they indicate how the mass density of the ith chemical species ρ_i, the velocity $\mathbf{v}$, and the total energy per unit mass $\hat{E}$ change in a small element of fluid which moves with the local fluid velocity (Bird [1] and Hirschfelder *et al.* [3].‡)

Eqs. of Continuity :

$$\frac{D\rho_i}{Dt} = -\rho_i(\nabla \cdot \mathbf{v}) - (\nabla \cdot \mathbf{j}_i) + r_{i\phi} \qquad i = 1, 2, 3, \ldots \nu \qquad (1)^*$$

‡ Explicit expressions for the various vector and tensor operations in cartesian coordinates are given at the end of the artiele.

* Addition of all ν equations of the form of eq. (1) gives :

$$\frac{D\rho}{Dt} = -\rho(\nabla \cdot \mathbf{v}) \qquad (1a)$$

which is the overall equation of continuity.

Eq. of Motion :

$$\rho \frac{D\mathbf{v}}{Dt} = -(\nabla \cdot \boldsymbol{\pi}) + \rho \hat{\mathbf{F}}_\phi \tag{2}$$

Eq. of Energy :

$$\rho \frac{D\hat{E}}{Dt} = -(\nabla \cdot \mathbf{q}) - \left(\nabla \cdot (\boldsymbol{\pi} \cdot \mathbf{v})\right) + \rho \hat{Q}_\phi \tag{3}\dagger$$

In the *second* form, derivable from the first, the equations are written so as to show them as laws of conservation of mass, momentum, and energy applied to a small volume element (fixed in space) through which the fluid is flowing :

Eq. of Continuity :

$$\frac{\partial}{\partial t}\rho_i = -\left(\nabla \cdot \{\rho_i \mathbf{v} + \mathbf{j}_i\}\right) + r_{i\phi} \tag{4}$$

Eq. of Motion :

$$\frac{\partial}{\partial t}\rho\mathbf{v} = -\left(\nabla \cdot \{\rho\mathbf{v}\,\mathbf{v} + \boldsymbol{\pi}\}\right) + \rho \hat{\mathbf{F}}_\phi \tag{5}$$

Eq. of Energy :

$$\frac{\partial}{\partial t}\rho\hat{E} = -\left(\nabla \cdot \{\rho\hat{E}\mathbf{v} + (\boldsymbol{\pi} \cdot \mathbf{v}) + \mathbf{q}\}\right) + \rho\hat{Q} \tag{6}$$

† Several alternate and completely equivalent formulations of the equation of energy balance are available ; one is in terms of internal energy and the other in terms of temperature :

$$\rho \frac{D\hat{U}}{Dt} = -(\nabla \cdot \mathbf{q}) - (\boldsymbol{\pi} : \nabla\mathbf{v}) + \rho\hat{Q}_\phi \tag{3a}$$

$$\rho\hat{C}_v \frac{DT}{Dt} = -(\nabla \cdot \mathbf{q}) - (\boldsymbol{\pi} : \nabla\mathbf{v}) + \rho\hat{Q}_\phi + \left(p - T\frac{\partial p}{\partial T}\right)(\nabla \cdot \mathbf{v}) + \sum_{i=1}^{v}\left[(\nabla \cdot \mathbf{j}_i) + r_{i\phi}\right]\left[\frac{\overline{U}_i}{M_i} + \left(p - T\frac{\partial p}{\partial T}\right)\frac{\overline{V}_i}{M_i}\right] \tag{3b}$$

in which the derivative $\partial p/\partial T$ is taken at constant composition and volume, and $\overline{U}_i$ and $\overline{V}_i$ are partial molal quantities. For single component, constant pressure systems eq. (3b) may be simplified to :

$$\rho\hat{C}_p \frac{DT}{Dt} = -(\nabla \cdot \mathbf{q}) - (\boldsymbol{\tau} : \nabla\mathbf{v}) + \rho\hat{Q}_\phi \tag{3c}$$

which is the basis for most engineering calculations. The term $(\boldsymbol{\tau} : \nabla\mathbf{v})$ is the heat produced by viscous dissipation (Lamb [4]) which may generally be neglected in flow problems.

The physical significance of the " microscopic balances " in eqs. (4), (5), and (6) is, term by term : The *equation of continuity* states that the local mass density of the ith species within a small region changes because of (i) the net influx of mass of i across the surface of the region by mass flow, (ii) the mass flux by diffusional processes (ordinary, thermal, pressure, and forced diffusion), and (iii) the production of the ith species by chemical reaction. The *equation of motion* states that the momentum within a small region changes because of (i) the flux of momentum across the surfaces by mass flow, (ii) the flux of momentum across the surfaces by pressure and viscous forces, and (iii) the external body forces (which are assumed to be the same for all species and derivable from a potential : $\hat{\mathbf{F}}_\phi = -\nabla\hat{\Phi}$). The *equation of energy* states that the total energy within a small region changes because of (i) the flux of energy across the surface by mass flow, (ii) the work done by the fluid in the region on its surroundings (both pressure-volume work and work asscociated with viscous forces), (iii) the flux of energy entering the system by heat conduction, radiation, and mass transfer, and (iv) the heat produced within the fluid by nuclear radiations.* Equations (4), (5), and (6) are all of the form :

(Accumulation) = (Input − Output) + (Production)

applied to a fixed differential volume element through which the fluid is flowing.

The equations of change together with boundary and initial conditions, the thermal equation of state ($\rho = \rho(p, T, \rho_i)$), and the caloric equation of state ($U = U(p, T, \rho_i)$) give the complete description of the flow system. In order to calculate concentration, velocity, and temperature profiles, one has to substitute expressions for $\mathbf{j}_i$, $\boldsymbol{\tau}$, and $\mathbf{q}$ in terms of the transport coefficients (coefficients of diffusion, viscosity, and thermal conductivity) and the gradients of the macroscopic

* The energy release accompanying chemical reaction is not included as a separate contribution in eqs. (3) and (6), inasmuch as it is inherently included in the internal energy contribution to $\hat{E}$. The heat of reaction does appear explicitly when the energy equation is rewritten in terms of temperature (see $r_{i\phi}$ terms in eq. (3b)).

properties (concentration, velocity, and temperature). The equations thereby obtained are useful for laminar flow calculations; their time-averaged counterparts are used as the starting point for turbulent flow calculations.

The equations of change written in eqs. (4), (5), and (6) may be integrated over the volume of any macroscopic engineering flow system, such as the one shown in Fig. 1. Thereby one obtains the macroscopic (or "overall") mass, momentum, and energy balances used in the analysis of engineering systems. One may also take the scalar product of $\mathbf{v}$ with the equation of motion in the form of eq. (2) and integrate the resulting equation over the volume of a macroscopic system to obtain the Bernoulli equation in the form usually used in engineering. It is well known that these overall balances give no information concerning the concentration, velocity, and temperature gradients in a system but simply connections between properties of the inlet and outlet streams.

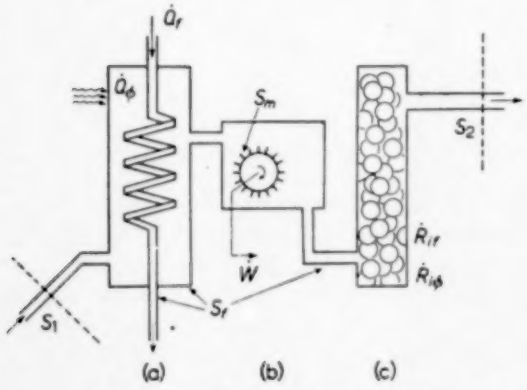

FIG. 1. Macroscopic flow system with mechanisms for (a) the addition of heat $\dot{Q}_f$ through fixed surface S_f and volume heat source $\dot{Q}_\phi$ resulting from subatomic radiations, (b) transfer of mechanical work $\dot{W}$ to surroundings by means of moving surface S_m, and (c) both homogeneous chemical reactions $\dot{R}_{i\phi}$ and heterogeneous (catalytic) reactions $\dot{R}_{if}$.

In the integration of the equations of change use is made of the Gauss divergence theorem to change the integration over the volume (V) of the divergence of a vector to an integral of the normal component of the vector over the system surface (S). In doing this three types of surfaces have to be distinguished: the fixed wetted solid surface in the system (S_f), the movable wetted surface which allows for the transfer of energy between the macroscopic system and its surroundings in the form of mechanical work (S_m), and the open end surfaces at the control surfaces (S_1, S_2). These different surfaces have to be treated individually. Throughout it is assumed that the fluid properties (e.g. density) do not vary appreciably over the control surfaces S_1 and S_2. The control surfaces are chosen in such a way that the flow velocity at S_1 and S_2 is, aside from turbulent fluctuations, parallel to the pipe axis and normal to the control surfaces. It is further assumed that transport of mass, momentum, and energy across S_1 and S_2 by molecular processes may be neglected in comparison with the transport by mass flow.

2. Macroscopic Mass Balance

Integration of eq. (4) over the volume of the macropscoic flow system V gives:*

$$\int_V \frac{\partial \rho_i}{\partial t}\, dV = -\int_V (\nabla \cdot \rho_i \mathbf{v})\, dV - \int_V (\nabla \cdot \mathbf{j}_i)\, dV + \int_V r_{i\phi}\, dV \quad (7)$$

The first two integrals on the right hand side may be transformed into surface integrals by means of the divergence theorem. The integral on the left hand side may be rewritten by taking the time derivative outside the integral sign. In so doing, however, one must remember that because of the moving parts within the flow system, the *shape* of the volume V is changing with time, and hence a term must be subtracted which accounts for the local gain or loss of mass by virtue of the motion of the surface. One thereby obtains:

* The mass flux $\mathbf{j}_i$ is the local flux of component i in gms cm^{-2} sec^{-1} referred to a co-ordinate system which is moving with the local mass average velocity $\mathbf{v}$. The relation of this flux to other fluxes (including the flux $\mathbf{N}_i$ more usual in chemical engineering) is given in ref. [1], Table III.

$$\frac{d}{dt}\int_V \rho_i dV - \int_S \rho_i v_{mn}\, dS = - \int_S \rho_i v_n\, dS - \int_S j_{in}\, dS + \int_V r_{i\phi}\, dV \quad (8)$$

Here v_n is the velocity of the *fluid* normal to the surface of the system, and v_{mn} is the component of the velocity of the moving *surface* which is normal to the surface (see Fig. 2). Hence eq. (8) becomes:

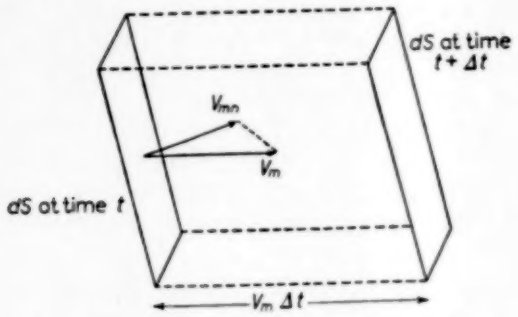

Fig. 2. A differential element of surface dS of the moving surface of the macroscopic system moves with an instantaneous velocity $\mathbf{v}_m$; the component of $\mathbf{v}_m$ normal to dS is v_{mn}.

$$\left.\begin{aligned}\dot{M}_i = &- \int_S \rho_i (v_n - v_{mn})\, dS \\ &- \int_{S_1+S_2} j_{in} dS - \int_{S_f} j_{in}\, dS + \int_V r_{i\phi}\, dV \\ &= (\rho_{i1}\bar{v}_1 S_1 - \rho_{i2}\bar{v}_2 S_2) \\ &- \int_{S_1+S_2} j_{in} dS + \dot{R}_{if} + \dot{R}_{i\phi}\end{aligned}\right\} \quad (9)\dagger$$

In the first term on the right hand side use has been made of the assumption that ρ_i is constant over the cross-section S_1 and S_2. The integral of j_{in} over S_1 and S_2 may be neglected in comparison with the first term which represents mass transport of the ith species by the overall flow motion. The integrals $\dot{R}_{if}$ and $\dot{R}_{i\phi}$ are the net rates of production of the ith species by surface reactions on S_f and by homogeneous reactions in the fluid phase respectively. If now $\dot{R}_i = \dot{R}_{if} + \dot{R}_{i\phi}$ and $\dot{J}_{i1} = \rho_{i1}\bar{v}_1 S_1$,

$$\dot{M}_i = -\Delta \dot{J}_i + \dot{R}_i \qquad i = 1, 2, \ldots \nu \quad (10)$$

where $\Delta \dot{J}_i = \dot{J}_{i2} - \dot{J}_{i1}$. Addition of all the ν equations represented by eq. (10) gives:

$$\dot{M} = -\Delta \dot{J} \quad (11)$$

Equations (10) and (11) are the familiar macroscopic mass balances for individual chemical species and for the fluid as a whole. For steady state operations $\dot{M}_i$ and $\dot{M}$ are zero.

3. Macroscopic Momentum Balance

Integration of eq. (5) over the volume gives:*

$$\left.\begin{aligned}\int_V \frac{\partial \rho \mathbf{v}}{\partial t}\, dV = &- \int_V (\nabla \cdot \rho \mathbf{vv})\, dV - \int_V \nabla p\, dV - \\ &\int_V (\nabla \cdot \boldsymbol{\tau})\, dV + \int_V \rho \hat{\mathbf{F}}_\phi\, dV\end{aligned}\right\} \quad (12)$$

The left hand side may be transformed as described in Section 2. And the first three volume integrals on the right hand side may be transformed into surface integrals by means of modifications of the divergence theorem (Milne-Thomson [5], Morse and Feshbach [6]).

† In what follows we use $\bar{v}$, $\overline{v^2}$, $\overline{v^3}$ for averages over a cross-sectional area; specifically for a circular tube these are defined by

$$\overline{v^n} = \int_0^{2\pi}\int_0^R v^n r\, dr\, d\theta \Big/ \int_0^{2\pi}\int_0^R r\, dr\, d\theta$$

where n is 1, 2, or 3.

* The element π_{xy} of the second-order pressure tensor $\boldsymbol{\pi}$ is the force per unit area acting in the x-direction on an elemental fluid surface perpendicular to the y-direction. The diagonal elements π_{xx}, π_{yy}, π_{zz} correspond to normal forces, and the non-diagonal elements $\pi_{xy} = \pi_{yx}$, $\pi_{xz} = \pi_{zx}$, and $\pi_{yz} = \pi_{zy}$ correspond to shearing forces. The diagonal elements include both hydrostatic pressure forces and viscous forces: $\pi_{xx} = p + \tau_{xx}$; the non-diagonal elements include only viscous forces: $\pi_{xy} = \tau_{xy}$. This is summarized by the tensor relation $\boldsymbol{\pi} = p\boldsymbol{\delta} + \boldsymbol{\tau}$, in which $\boldsymbol{\delta}$ is the unit tensor ($\delta_{xx} = \delta_{yy} = \delta_{zz} = 1$, all other components are zero). In eq. (12) $\boldsymbol{\pi}$ is split up into p and $\boldsymbol{\tau}$ and use is made of the fact that $(\nabla : \boldsymbol{\pi}) = \nabla p + (\nabla : \boldsymbol{\tau})$.

$$\left.\begin{aligned}\frac{d}{dt}\int_V \rho\mathbf{v}\,dV = &-\int_S \rho\mathbf{v}\,(v_n - v_{mn})\,dS - \\ &\int_S p\mathbf{n}\,dS - \int_S (\boldsymbol{\tau}\cdot\mathbf{n})\,dS + \int_V \rho\hat{\mathbf{F}}_\phi\,dV\end{aligned}\right\} \quad (13)$$

Here $\mathbf{n}$ is the normal unit vector directed outwardly from the system surface. The left hand side is the time rate of change of the total momentum $\mathbf{P}$ of the fluid in the system. The first term on the right hand side vanishes on all solid surfaces; the contribution at S_1 and S_2 represents the rate of flow of momentum into and out of the system by virtue of fluid flow alone. The second term on the right gives a contribution to the influx and efflux of momentum due to pressure forces at S_1 and S_2, and also a contribution to the drag force on the equipment on S_f and S_m. The third term also contributes to the drag force on the equipment due to viscous forces on the solid surfaces S_f and S_m; in addition this term includes momentum transport into and out of the system at S_1 and S_2 by viscous action – a contribution almost always safely neglected. The fourth term gives the total force exerted on the fluid in the system by external body forces such as gravity. Hence one obtains finally the macroscopic momentum balance:

$$\dot{\mathbf{P}} = -\Delta(\rho\overline{v^2}\,\mathbf{S} + p\mathbf{S}) - \mathbf{F}_{\text{drag}} + \mathbf{F}_{\text{ext}} \quad (14)$$

or in terms of the mass rate of flow:

$$\dot{\mathbf{P}} = -\Delta\left(\frac{\overline{v^2}}{\bar{v}}\,\dot{\mathbf{J}} + p\mathbf{S}\right) - \mathbf{F}_{\text{drag}} + \mathbf{F}_{\text{ext}} \quad (15)$$

Here $\mathbf{S}$ indicates a vector whose magnitude is the surface area of the cross section and whose direction is normal to the cross-section (chosen to point in the direction of flow!). The vector $\dot{\mathbf{J}}$ is the mass rate of flow vector similarly defined. The negative of $\mathbf{F}_{\text{drag}}$ is just the "reaction force" offered by the equipment. Note that the average value of the square of the velocity appears properly in the momentum balance (Rouse and Howe [7]).

4. Macroscopic Energy Balance

Integration of eq. (6) over V gives:

$$\left.\begin{aligned}\int_V \frac{\partial\rho\hat{E}}{\partial t}\,dV = &\\ -\int_V (\nabla\cdot\rho\hat{E}\mathbf{v})\,dV - &\int_V (\nabla\cdot(\boldsymbol{\pi}\cdot\mathbf{v}))\,dV \\ -\int_V (\nabla\cdot\mathbf{q})\,dV + &\int_V \rho\hat{Q}_\phi\,dV\end{aligned}\right\} \quad (16)$$

The first three volume integrals on the right hand side may be transformed into surface integrals as before.

$$\left.\begin{aligned}\frac{d}{dt}\int_V \rho\hat{E}\,dV = &\\ -\int_S \rho\hat{E}\,(v_n - v_{mn})\,dS - &\int_S (\boldsymbol{\pi}\cdot\mathbf{v})_n\,dS \\ -\int_{S_f} q_n\,dS + &\int_V \rho\hat{Q}_\phi\,dV\end{aligned}\right\} \quad (17)$$

The left hand side is the rate of change of the total energy in the system. On the right hand side the first integral is zero except on S_1 and S_2 and represents the energy flowing in and out with the fluid. The second integral vanishes on S_f; its value on S_m gives the rate at which work is done on the external surroundings, $\dot{W}$, resulting from both pressure and viscous forces on the moving parts: on S_1 and S_2 it contains a term pv_n (the pressure-volume work) and a term $(\boldsymbol{\tau}\cdot\mathbf{v})_n$ (the shear work), the latter being generally neglected. The third integral gives the heat added to the system over the solid surface $\dot{Q}_f$; there is also a contribution at S_1 and S_2 which represents the heat input and outflow by conduction in the fluid stream, this contribution generally being quite small in comparison with the heat transport by bulk flow. Finally the fourth integral represents the volume heat production $\dot{Q}_\phi$. The surface integral over $\hat{E}$ can be shown as being made up of internal energy $\hat{U}$, kinetic energy $\frac{1}{2}v^2$, and potential energy $\hat{\Phi}$ (all on a per unit mass basis). Then eq. (17) finally becomes:

$$\left.\begin{aligned}\dot{E} = -\Delta(\rho\hat{U}\bar{v}S + \tfrac{1}{2}\rho\overline{v^3}S + \rho\bar{v}\,\hat{\Phi}S + p\bar{v}S)&\\ + \dot{Q} - \dot{W}&\end{aligned}\right\} \quad (18)$$

in which $\dot{E} = \dot{U} + \dot{K} + \dot{\Phi}$ and $\dot{Q} = \dot{Q}_f + \dot{Q}_\phi$. Or, in terms of the mass rate of flow, the macroscopic energy balance is :

$$\dot{E} = -\Delta(\hat{U} + p\hat{V} + \tfrac{1}{2}(\overline{v^3}/\overline{v}) + \hat{\Phi})\,\dot{J} + \dot{Q} - \dot{W} \quad (19)^*$$

Here it is seen that the average value of the cube of the velocity enters quite naturally (Rouse and Howe [7]).

5. The "Engineering Bernoulli Equation"

The formation of the scalar product of $\mathbf{v}$ with eq. (2) gives (Streeter [8]) after some manipulation :

$$\left.\begin{aligned}\rho \frac{D}{Dt}(\tfrac{1}{2}v^2) = &-(\mathbf{v}\cdot\nabla p)\\ &-\big(\mathbf{v}\cdot(\nabla\cdot\boldsymbol{\tau})\big) + \rho(\mathbf{v}\cdot\hat{\mathbf{F}}_\phi)\end{aligned}\right\} \quad (20)$$

This is an energy equation involving only mechanical terms – that is, heat and internal energy do not appear. The left hand side may be rewritten by using the equation of continuity to give terms (a) and (b) below ; and the second term on the right hand side may be split up into two terms (d) and (e), provided that use is made of the fact that $\boldsymbol{\tau}$ is a symmetric tensor. Thereby one obtains :

$$\left.\begin{aligned}\underset{(a)}{\frac{\partial}{\partial t}(\tfrac{1}{2}\rho v^2)} = &-\underset{(b)}{(\nabla\cdot\tfrac{1}{2}\rho v^2\,\mathbf{v})} - \underset{(c)}{(\mathbf{v}\cdot\nabla p)}\\ &-\underset{(d)}{(\nabla\cdot(\boldsymbol{\tau}\cdot\mathbf{v}))} + \underset{(e)}{(\boldsymbol{\tau}:\nabla\mathbf{v})} + \underset{(f)}{\rho(\mathbf{v}\cdot\hat{\mathbf{F}}_\phi)}\end{aligned}\right\} \quad (21)$$

* For *steady-state* $\dot{J}_1 = \dot{J}_2$ and eq. (19) can be written on a per unit mass basis by dividing through by $\dot{J}$.

$$\Delta(\hat{U} + p\hat{V} + \tfrac{1}{2}(\overline{v^3}/\overline{v}) + \hat{\Phi}) = \hat{Q} - \hat{W} \quad (19a)$$

It should be noted that $\hat{Q}$ does not include the heat produced by chemical reaction inasmuch as that effect is automatically included in the calculation of the internal energies $\hat{U}_1$ and $\hat{U}_2$ of the inlet and outlet streams.

This equation is next integrated over V to give :

Term (a) :

$$\left.\begin{aligned}\int_V \frac{\partial}{\partial t}(\tfrac{1}{2}\rho v^2)\,dV = &\\ \frac{d}{dt}\int_V \tfrac{1}{2}\rho v^2 dV - \int_S (\tfrac{1}{2}\rho v^2)\,v_{mn}\,dS &\\ = \dot{K} - \int_{S_m} (\tfrac{1}{2}\rho v^2)\,v_{mn}\,dS &\end{aligned}\right\} \quad (22)$$

Here $\dot{K}$ is the rate of change of the total kinetic energy within the system

Term (b) :

$$\left.\begin{aligned}-\int_V (\nabla\cdot\tfrac{1}{2}\rho v^2\mathbf{v})\,dV &= \int_{S_1,S_2} \tfrac{1}{2}\rho v^2 v_n dS\\ &\quad - \int_{S_m} \tfrac{1}{2}\rho v^2 v_n dS\\ &= -\Delta(\tfrac{1}{2}\rho\overline{v^3}S) - \int_{S_m} \tfrac{1}{2}\rho v^2 v_{mn}\,dS\\ &= -\Delta\left(\tfrac{1}{2}\frac{\overline{v^3}}{\overline{v}}\,\dot{J}\right) - \int_{S_m} \tfrac{1}{2}\rho v^2 v_{mn} dS\end{aligned}\right\} \quad (23)$$

The integral over S_m just cancels the same integral in eq. (22) ; the other term gives the input of kinetic energy at surface 1 minus the output at surface 2.

Term (d) :

$$-\int_V (\nabla\cdot(\boldsymbol{\tau}\cdot\mathbf{v}))\,dV = -\int_{S_m} (\boldsymbol{\tau}\cdot\mathbf{v})_n\,dS = -\dot{W}_v \quad (24)$$

The contributions of the surface integral over S_1 anc S_2 are neglected as was done in going from eq. (17) to eq. (18) ; $\dot{W}_v$ is the rate of transferring mechanical energy to the surroundings because of the viscous forces.

Term (*e*) :

$$+\int_V (\boldsymbol{\tau} : \nabla \mathbf{v})\, dV = -\dot{E}_v \qquad (25)$$

This is the total rate of energy loss by viscous dissipation within the system (LAMB [4]) – that is, the friction losses resulting from the degradation of mechanical energy into heat.

Term (*f*) may be evaluated by introducing the potential energy, which is related to $\hat{\mathbf{F}}_\phi$ by $\hat{\mathbf{F}}_\phi = -\nabla\hat{\Phi}$:

$$\int_V (\rho\mathbf{v}\cdot\hat{\mathbf{F}}_\phi)\, dV = -\int_V (\rho\mathbf{v}\cdot\nabla\hat{\Phi})\, dV$$
$$= -\int_V (\nabla\cdot\rho\mathbf{v}\,\hat{\Phi})\, dV + \int_V \hat{\Phi}\,(\nabla\cdot\rho\mathbf{v})\, dV$$

The first of these integrals may be transformed by using the divergence theorem and the second may be rewritten by using the equation of continuity (and the fact that $\hat{\Phi}$ is time-independent) :

$$\left.\begin{aligned} &-\int_S \rho v_n \hat{\Phi} dS - \int_V \hat{\Phi}\frac{\partial\rho}{\partial t}\, dV \\ &\quad = -\int_S \rho v_n \hat{\Phi} dS \\ &\qquad - \frac{d}{dt}\int_V \rho\hat{\Phi} dV + \int_S \rho\hat{\Phi} v_{mn} dS \\ &\quad = -\int_S \rho\hat{\Phi}\,(v_n - v_{mn})\, dS - \dot{\Phi} \\ &\quad = -\Delta\,(\rho\bar{v}\hat{\Phi}S) - \dot{\Phi} \\ &\quad = -\Delta\,(\hat{\Phi}\dot{J}) - \dot{\Phi} \end{aligned}\right\} \qquad (26)$$

The first term is just the influx and efflux of potential energy, and $\dot{\Phi}$ is the rate of change of the potential energy of the entire system.

Term (*c*) requires special consideration. If the fluid is of constant temperature and composition, then use can be made of the fact that $(1/\rho)dp = d\hat{G}$ and the development parallels the treatment of term (*f*) :

$$\left.\begin{aligned} &-\int_V (\mathbf{v}\cdot\nabla p)\, dV \\ &\quad = -\int_V (\rho\mathbf{v}\cdot\frac{1}{\rho}\nabla p)\, dV \\ &\quad = -\int_V (\rho\mathbf{v}\cdot\nabla\hat{G})\, dV \\ &\quad = -\int_S \rho\mathbf{v}_n\hat{G} dS - \int_V \hat{G}\frac{\partial\rho}{\partial t}\, dV \\ &\quad = -\int_S \rho v_n \hat{G} dS - \frac{d}{dt}\int_V \rho\hat{G} dV \\ &\qquad + \int_S \rho\hat{G} v_{mn}\, dS + \int_V \frac{\partial p}{\partial t}\, dV \\ &\quad = -\int_S \rho\hat{G}\,(v_n - v_{mn})\, dS \\ &\qquad - \frac{d}{dt}\int_V (\rho\hat{G} - p)\, dV - \int_S p v_{mn} dS \\ &\quad = -\Delta\,(\rho\hat{G}\bar{v}S) - \dot{A} - \dot{W}_p \\ &\quad = -\Delta\,(\hat{G}\dot{J}) - \dot{A} - \dot{W}_p \end{aligned}\right\} \qquad (27)$$

The first term gives the rate of influx and efflux of $\hat{G}$; the second term is the time rate of change of the Helmholtz free energy $A = G - pV$ for the whole system ; and the third term is the work done by pressure forces on the moving parts.

Combination of the results of eqs. (21) through (27) gives then finally :

$$\dot{K} + \dot{\Phi} + \dot{A} = -\Delta\left(\tfrac{1}{2}\frac{\overline{v^3}}{\bar{v}} + \hat{\Phi} + \hat{G}\right)\dot{J} - \dot{W} - \dot{E}_v \qquad (28)$$

where $\dot{W} = \dot{W}_v + \dot{W}_p$. This is the unsteady state engineering Bernoulli equation for an isothermal system of constant chemical composition.

For an isentropic system of constant composition, term (*c*) is evaluated by noting that $(1/\rho)dp = d\hat{H}$. A similar procedure leads to the result

$$\dot{K} + \dot{\Phi} + \dot{U} = -\Delta\left(\tfrac{1}{2}\frac{\overline{v^3}}{\bar{v}} + \hat{\Phi} + \hat{H}\right)\dot{J} - \dot{W} - \dot{E}_v \qquad (29)$$

For a system which is neither isothermal nor isentropic or in which chemical reactions are taking place no such simple results may be

written down. The two cases described by eqs. (28) and (29) are those usually considered in engineering text (Coulson and Richardson [2]).

For steady state operation $\dot{J}_1 = \dot{J}_2 = \dot{J}$, and the engineering Bernoulli equation may be written on a per unit mass basis by dividing through by $\dot{J}$ to obtain :

$$\Delta \tfrac{1}{2} \frac{\overline{v^3}}{\bar{v}} + \Delta \hat{\Phi} + \int_{p_1}^{p_2} \frac{dp}{\rho} + \hat{W} + \hat{E}_v = 0 \qquad (30)$$

For the isothermal, constant-composition process the line integral reduces to $\Delta \hat{G}$; for the isentropic, constant-composition process the line integral is $\Delta \hat{H}$. For any other process the best one can do is to evaluate the line integral over the succession of thermodynamic states encountered in the flow from S_1 to S_2, the integration being performed over some representative streamline in the system. This implies that one know, for example, how ρ varies with p, T, and composition (specification of the equation of state) and how T and the composition vary with p (specification of the path of the line integral).

Acknowledgement—The author wishes to acknowledge the Wisconsin Alumni Research Foundation for financial support during the course of this work. He also desires to thank Professor C. F. Curtiss and Mr. L. B. Rothfeld (University of Wisconsin), Professor J. M. Smith (Purdue University), Professor H. G. Drickamer (University of Illinois), and Professor W. E. Ranz (Pennsylvania State University), for reading the manuscript and offering numerous suggestions.

Notation

A = Helmholtz free energy
C_p = heat capacity at constant pressure
C_v = heat capacity at constant volume
E = total energy
E_v = energy loss due to friction
$\mathbf{F}_\phi$ = volume force $= -\nabla\Phi$
$\mathbf{F}_{ext}$ = total external force
$\mathbf{F}_{drag}$ = total drag force
G = Gibbs free energy $= A + pV$
H = enthalpy
$\mathbf{j}_i$ = mass flux of ith component with respect to the mass average flow velocity ($\Sigma]_i = 0$)
$\dot{J}$ = mass rate of flow
K = total kinetic energy of macroscopic system
M = total mass of fluid in macroscopic system
M_i = mass of the ith species in the macroscopic flow system
$\mathbf{n}$ = outwardly directed normal unit vector
p = static pressure
$\mathbf{P}$ = total momentum of system
$\mathbf{q}$ = heat flux vector
q_n = normal component of $\mathbf{q}$
Q_f = heat transferred across surface of macroscopic system
Q_ϕ = volume heat source in macroscopic system
$r_{i\phi}$ = mass of ith chemical species produced by homogeneous chemical reaction ($\Sigma r_i = 0$)
$\dot{R}_i$ = total rate of production of mass of the ith species in the macroscopic system
S = surface of flow system
S_f, S_m = fixed and moving surfaces of the system
S_1, S_2 = cross-sectional area of flow system at 1, 2
t = time
U = internal energy
$\mathbf{v}$ = velocity
v_n = normal component of v
V = volume of flow system
$\bar{v}$ = velocity averaged over a cross-section
$\mathbf{v}_m$ = velocity of surface of a moving part
v_{mn} = normal component of $\mathbf{v}_m$
W = work done by system on its surroundings
W_v = work resulting from pressure forces, viscous forces on moving parts of the equipment
Δ = quantity evaluated at S_2 minus quantity evaluated at S_1
$\boldsymbol{\delta}$ = unit tensor
$\boldsymbol{\pi} = p\boldsymbol{\delta} + \boldsymbol{\tau}$ = pressure tensor
ρ = mass density $= (1/\hat{V}) = \Sigma\rho_i$
ρ_i = mass density of ith chemical species
$\boldsymbol{\tau}$ = shear stress tensor
Φ = potential energy

Marks above symbols :

$\hat{}$ = quantity per unit mass of fluid
$\bar{}$ = quantity averaged over cross-section of flow system
$\cdot$ = time rate of change of quantity, pertaining to the macroscopic system

Subscripts :

f = quantity associated with fixed surface
m = quantity associated with moving surface
ϕ = quantity associated with the fluid
n = normal component of a vector
v = quantity associated with viscous effects
p = quantity associated with pressure effects
i = ith chemical species

*Vector and Tensor Operations in Cartesian Co-ordinates**

Scalars are indicated by light face symbols

Vectors are indicated by **bold face Roman** symbols

Tensors are indicated by **bold face Greek** symbols

$\mathbf{i}, \mathbf{j}, \mathbf{k}$ = unit vectors in x, y, z directions

$\mathbf{v} = \mathbf{i}v_x + \mathbf{j}v_y + \mathbf{k}v_z$ = vector with 3 components v_x, v_y, v_z

$\boldsymbol{\tau}$ = second order tensor with 9 components τ_{xx}, τ_{xy}, τ_{xz}, etc.†

$\mathbf{vv}$ = dyadic product with 9 components v_xv_x, v_xv_y, v_xv_z, etc.

$v^2 = (\mathbf{v} \cdot \mathbf{v}) = v_x^2 + v_y^2 + v_z^2$

$(\mathbf{v} \cdot \mathbf{w}) = v_xw_x + v_yw_y + v_zw_z$ = scalar product of two vectors

$(\boldsymbol{\tau} \cdot \mathbf{v})_x = \tau_{xx}v_x + \tau_{xy}v_y + \tau_{xz}v_z$

$\boldsymbol{\delta}$ = second order unit tensor with three components $\delta_{ii} = 1$ and six components $\delta_{ij} = 0$ $(i \neq j)$

$$\nabla p = \mathbf{i}\frac{\partial p}{\partial x} + \mathbf{j}\frac{\partial p}{\partial y} + \mathbf{k}\frac{\partial p}{\partial z} = \text{the "gradient of } p\text{"}$$

$$(\nabla \cdot \mathbf{v}) = \frac{\partial v_x}{\partial x} + \frac{\partial v_y}{\partial y} + \frac{\partial v_z}{\partial z} = \text{the "divergence of } \mathbf{v}\text{"}$$

$$(\nabla \cdot \boldsymbol{\tau})_x = \frac{\partial \tau_{xx}}{\partial x} + \frac{\partial \tau_{yx}}{\partial y} + \frac{\partial \tau_{zx}}{\partial z}$$

$$(\nabla \cdot \rho\mathbf{vv})_x = \frac{\partial}{\partial x}\rho v_xv_x + \frac{\partial}{\partial y}\rho v_yv_x + \frac{\partial}{\partial z}\rho v_zv_x$$

$$(\mathbf{v} \cdot \nabla)p = (\mathbf{v} : \nabla p) = v_x\frac{\partial p}{\partial x} + v_y\frac{\partial p}{\partial y} + v_z\frac{\partial p}{\partial z}$$

$$(\boldsymbol{\tau} : \nabla\mathbf{v}) = \sum_\alpha \sum_\beta \tau_{\alpha\beta}(\partial v_\alpha/\partial x_\beta) \qquad (\alpha, \beta = x, y, z)$$

$\nabla\mathbf{v}$ = dyadic product with nine components $\partial v_x/\partial x$, $\partial v_y/\partial x$, $\partial v_z/\partial x$, $\partial v_x/\partial y$, etc.

$$\frac{D\rho}{Dt} = \frac{\partial p}{\partial t} + (\mathbf{v} \cdot \nabla)\rho = \text{the "substantial derivative of } \rho\text{"}$$

* See ref. [1] for a tabulation of the more difficult operations in cyclindrical and spherical co-ordinates.

† All tensors used in this article are "symmetric" – that is $\tau_{ij} = \tau_{ji}$.

References

[1] Bird R. B. Theory of Diffusion, Chapter in *Advances in Chemical Engineering*, I, Academic Press, New York (1956) 155-238.

[2] Coulson J. M. and Richardson J. F. *Chemical Engineering*, McGraw-Hill, New York (1954) Vol. I, 24-27.

[3] Hirschfelder J. O., Curtiss C. F., and Bird R. B. *Molecular Theory of Gases and Liquids*, Wiley, New York (1954) Sections 7.2e, 9.4d, 11.1b.

[4] Lamb H. *Hydrodynamics*, Cambridge University Press, 6th ed. (1932) 579-581.

[5] Milne-Thomson L. M. *Theoretical Hydrodynamics*, Macmillan, New York, 3rd ed. (1955) 51-52.

[6] Morse P. M. and Feshbach H. *Methods of Theoretical Physics*, McGraw-Hill, New York (1953) 65-66.

[7] Rouse H. and Howe J. W. *Basic Mechanics of Fluids*, Wiley, New York (1953) 71, 78.

[8] Streeter V. L. *Fluid Dynamics*, McGraw-Hill, New York (1948) 23-26 (see also ref. [4], p. 21).

Chemical Engineering Science, 1957, Vol. 6, pp. 132 to 137. Pergamon Press Ltd.

Compressibility, fugacity, and water-solubility of carbon dioxide in the region 0-36 atm. and 0-100°c

G. Houghton, A. M. McLean, and P. D. Ritchie

Technical Chemistry Department, Royal College of Science and Technology, Glasgow

(*Received 5 September* 1956)

Abstract—An improved form of the Beattie volume-explicit equation of state for carbon dioxide is described, containing two additional terms. Tables of compressibility, fugacity, and water-solubility of carbon dioxide are presented for the region 0–36 atm. and 0–100°C.

Résumé—L'auteur présente une forme améliorée de l'équation explicite d'état de Beattie, équation d'étar du gaz carbonique avec deux termes additionnels. Il donne des tables de compressibilité, fugacité et solubilité de l'eau de l'anhydride carbonique pour les régions de 0–36 atm. et 0–100°C.

Introduction

For the design of a carbon dioxide absorber operating at pressures up to 36 atm. [1] it has been found necessary to revise existing data on the compressibility, fugacity, and water-solubility of carbon dioxide for pressures in the range 0–36 atm. and temperatures in the range 0–100°C. It is hoped that the revised data in this paper will prove useful to other workers.

To calculate the fugacity it was necessary to obtain an equation of state, explicit in volume. The only volume-explicit equation available in the literature for the required range of temperature and pressure was the Beattie equation [2], which had been obtained by inversion of the Beattie-Bridgeman pressure-explicit equation [3]. Both equations were based upon the data of Andrews [4] for the compressibility of carbon dioxide. When the Beattie equation was tested by using the more recent compressibility data of Michels and Michels [5], the average deviation of the calculated from the experimental volumes was 2·4%, much too great an error for the accurate computations now required.

Zelvinskii [6] determined the water-solubility of carbon dioxide at certain temperatures in the range 0–100°C and pressures up to 90 atm., while Wiebe and Gaddy [7] gave the solubilities of carbon dioxide for a single pressure (25 atm.) within the range now required, and at seven temperatures between 18° and 100°C. There are, in addition, the solubility data (1 atm.) of Bohr and Bock [8], quoted in most handbooks. Since all these data are expressed in different units, it was decided (i) to evaluate their accuracy and compile a table of solubilities suitable for design purposes, and (ii) to test the validity of Henry's law (and its fugacity correction) so that the chemical engineer might have a guide to the use of this law for the system carbon dioxide-water.

Equation of State for Carbon Dioxide

Andrews [4] obtained his data by comparing the volumes of carbon dioxide and air at the same temperature and pressure. The compressibility of air was unknown in 1876, and Andrews assumed it to be unity; however, it was possible to refine his data by applying a correction for the compressibility of air, using the data of Holborn and Otto [9]. Based upon the corrected Andrews' data, the volumes calculated from the Beattie equation had an average deviation of 1·6%, with a maximum of 6·6%.

A review of equations of state shows that volume-explicit equations require more empirical constants than pressure-explicit equations to achieve the same accuracy. The Beattie equation has therefore been modified, by the addition of two further terms, to fit the more recent experimental data [5]. It can be expanded into the following volume-explicit form :

$$V = 0{\cdot}10476 + \frac{RT}{P} - \frac{61{\cdot}0102}{T} - \frac{660{,}000}{T^3} - \frac{P}{RT}\left[0{\cdot}007579 - \frac{4{\cdot}35126}{T} + \frac{69141{\cdot}6}{T^3}\right] + \left(\frac{P}{RT}\right)^3\left[\frac{5002{\cdot}39}{T^3}\right] \quad (1)$$

When the most recent compressibility data for carbon dioxide [5] are used to test equation (1) the calculated molal volumes show an average deviation of 2·4%, and a maximum deviation of 11·7%, from the experimental values. Further, the deviations are such that the calculated volumes are always larger than the experimental. Graphical and analytical examination of these deviations has now shown that the BEATTIE equation can be adjusted to fit the MICHELS and MICHELS data by the addition of two further empirical terms. The deviations are found to be a function of both temperature and pressure; hence, one term, $-2{\cdot}47 \times 10^{27}/T^{12}$, is now added to allow for the temperature effect, and a second term $-(P/RT)^2(2{\cdot}69354 \times 10^{10}/T^5)$ to allow for the combined effects of temperature and pressure. This leads to the following volume-explicit equation:

$$V = 0{\cdot}10476 + \frac{RT}{P} - \frac{61{\cdot}0102}{T} - \frac{660{,}000}{T^3} - \frac{2{\cdot}47 \times 10^{27}}{T^{12}} - \frac{P}{RT}\left[0{\cdot}007579 - \frac{4{\cdot}35126}{T} + \frac{69141{\cdot}6}{T^3}\right] + \left(\frac{P}{RT}\right)^2\left[\frac{5002{\cdot}39}{T^3} - \frac{2{\cdot}69354 \times 10^{10}}{T^5}\right] \quad (2)$$

Equation (2) can be converted into the compressibility form by multiplying through by P/RT to obtain:

$$Z = \frac{PV}{RT} - 1 + \frac{P}{RT}\left[0{\cdot}10476 - \frac{61{\cdot}0102}{T} - \frac{660{,}000}{T^3} - \frac{2{\cdot}47 \times 10^{27}}{T^{12}}\right] - \left(\frac{P}{RT}\right)^2\left[0{\cdot}007579 - \frac{4{\cdot}35126}{T} + \frac{69141{\cdot}6}{T^3}\right] + \left(\frac{P}{RT}\right)^3\left[\frac{5002{\cdot}39}{T^3} - \frac{2{\cdot}69354 \times 10^{10}}{T^5}\right] \quad (3)$$

These equations of state can be applied to carbon dioxide, over the pressure range 0–36 atm. and the temperature range 3–100°C, with an average deviation of 0·17% and a maximum deviation of 0·35%. They can also be applied, with the same deviations, over the temperature range 0–3°C and the pressure range 0–33·4 atm. The vapour pressure of liquid carbon dioxide at 0°C is 33·4 atm., so that within the narrow range 0–3°C the substance will be liquid at pressures above 33·4 atm. Equations (2) and (3) have been derived solely for the purpose of interpolation so that accurate compressibility coefficients could be tabulated. These coefficients are given in the Table at equal temperature and pressure increments.

It should be noted that equations (2) and (3) also agree well with the older ANDREWS data [4], with an average deviation of 0·38% and a maximum deviation of 0·53%. However, the deviations are always positive, indicating that there is some constant error in the ANDREWS data which makes the volumes consistently smaller than those reported by MICHELS and MICHELS.

COMPRESSIBILITY

The compressibility of carbon dioxide, as calculated from equation (3), is given in the Table for pressure increments of 2 atm. up to 36 atm., and for temperatures of 0°, 10°, 15°, 20°, 25°, 35°, 50°, 75° and 100°C. For design purposes, intermediate values can be interpolated; alternatively, a compressibility chart can be constructed.

FUGACITY

The fugacity coefficient of carbon dioxide is obtained by substituting equation (2) into the following integral:

$$\ln f = \int_0^P \frac{V}{RT}\,dP \quad (4)$$

The resulting definite integral is integrated term by term to obtain the following expression for the fugacity coefficient:

$$\ln \frac{f}{P} = \frac{P}{RT}\left[0{\cdot}10476 - \frac{61{\cdot}0102}{T} - \frac{660{,}000}{T^3} - \frac{2{\cdot}47 \times 10^{27}}{T^{12}}\right] - \left(\frac{P}{RT}\right)^2 \left[0{\cdot}0037895 - \frac{2{\cdot}17563}{T} + \frac{34570{\cdot}8}{T^3}\right] + \left(\frac{P}{RT}\right)^3 \left[\frac{1667{\cdot}46}{T^3} - \frac{8{\cdot}97847 \times 10^9}{T^5}\right] \quad (5)$$

The fugacity coefficients (f/P) calculated from equation (5) are summarised in the Table.

Water-Solubility of Carbon Dioxide

Before the results of Zelvinskii [6], Wiebe and Gaddy [7], and Bohr and Bock [8] can be compared, all the data must be converted into the same units of solubility. The units used here are the Bunsen absorption coefficient (α), and the mole fraction of dissolved carbon dioxide (x).

Table 1. *Compressibility, Fugacity, and Water-Solubility of Carbon Dioxide*

$Z = PV/RT$ = compressibility coefficient; f/P = fugacity coefficient;

α = Bunsen absorption coefficient, volume of gas calculated at N.T.P. dissolved by 1 volume of water at a certain temperature and partial pressure P of CO_2;

x = mol. fraction of dissolved CO_2 in water at a certain temperature and partial pressure P of CO_2.

P (atm.)	0°C				10°C			
	Z	f/P	α	$x \times 10^3$	Z	f/P	α	$x \times 10^3$
1	0·99263	0·99266	1·800	1·445	0·99359	0·99362	1·218	0·985
2	0·98527	0·98536	3·58	2·89	0·98719	0·98724	2·41	1·946
4	0·97055	0·97098	6·96	5·60	0·97440	0·97470	4·71	3·80
6	0·95576	0·95676	10·14	8·14	0·96156	0·96230	6·91	5·56
8	0·94082	0·94275	13·12	10·51	0·94862	0·95004	9·00	7·23
10	0·92567	0·92886	15·90	12·71	0·93554	0·93788	10·98	8·81
12	0·91022	0·91512	18·48	14·74	0·92224	0·92584	12·86	10·30
14	0·89440	0·90146	20·86	16·60	0·90868	0·91388	14·63	11·70
16	0·87814	0·88792	23·04	18·31	0·89480	0·90198	16·29	13·02
18	0·86136	0·87442	25·02	19·85	0·88054	0·89016	17·85	14·24
20	0·84400	0·86097	26·80	21·23	0·86585	0·87836	19·30	15·38
22	0·82596	0·84753	28·38	22·46	0·85068	0·86657	20·64	16·44
24	0·80719	0·83413	29·76	23·52	0·83495	0·85483	21·88	17·41
26	0·78760	0·82073	30·94	24·43	0·81863	0·84305	23·01	18·29
28	0·76712	0·80731	31·92	25·19	0·80166	0·83130	24·04	19·09
30	0·74567	0·79387	32·70	25·79	0·78397	0·81950	24·96	19·80
32	0·72319	0·78039	33·28	26·23	0·76552	0·80770	25·77	20·44
34	—	—	—	—	0·74624	0·79583	26·48	20·98
36	—	—	—	—	0·72608	0·78393	27·08	21·45
	15°C				20°C			
1	0·99400	0·99400	0·990	0·802	0·99437	0·99436	0·855	0·692
2	0·98800	0·98806	1·963	1·587	0·98874	0·98880	1·697	1·374
4	0·97602	0·97630	3·86	3·11	0·97750	0·97772	3·35	2·70
6	0·96401	0·96464	5·68	4·58	0·96624	0·96678	4·94	3·99
8	0·95193	0·95314	7·43	5·98	0·95491	0·95596	6·50	5·24
10	0·93971	0·94174	9·10	7·32	0·94348	0·94524	8·00	6·44
12	0·92732	0·93042	10·71	8·60	0·93190	0·93458	9·45	7·60
14	0·91470	0·91918	12·25	9·82	0·92013	0·92402	10·85	8·72
16	0·90181	0·90796	13·72	10·99	0·90812	0·91350	12·21	9·81
18	0·88860	0·89690	15·11	12·09	0·89584	0·90302	13·52	10·84
20	0·87501	0·88580	16·43	13·13	0·88324	0·89258	14·78	11·84
22	0·86101	0·87474	17·68	14·12	0·87029	0·88218	15·99	12·80
24	0·84654	0·86370	18·86	15·05	0·85693	0·87178	17·13	13·70
26	0·83156	0·85263	19·97	15·92	0·84312	0·86140	18·26	14·59
28	0·81601	0·84160	21·01	16·73	0·82883	0·85100	19·32	15·43
30	0·79985	0·83053	21·99	17·49	0·81401	0·84058	20·34	16·22
32	0·78303	0·81941	22·87	18·19	0·79862	0·83013	21·30	16·98
34	0·76549	0·80830	23·69	18·83	0·78262	0·81967	22·22	17·70
36	0·74720	0·79713	24·45	19·42	0·76596	0·80917	22·99	18·30

Table 1. (*continued*)

P (*atm.*)	25°C				35°C			
	Z	*f*/*P*	α	$x \times 10^3$	Z	*f*/*P*	α	$x \times 10^3$
1	0·99470	0·99472	0·749	0·608	0·99529	0·99532	0·581	0·473
2	0·98941	0·98946	1·489	1·207	0·99060	0·99062	1·159	0·943
4	0·97885	0·97904	2·95	2·39	0·98121	0·98136	2·30	1·868
6	0·96827	0·96874	4·37	3·53	0·97183	0·97218	3·42	2·78
8	0·95764	0·95854	5·76	4·65	0·96241	0·96310	4·52	3·67
10	0·94691	0·94844	7·11	5·74	0·95293	0·95410	5·60	4·54
12	0·93607	0·93840	8·43	6·80	0·94337	0·94516	6·66	5·39
14	0·92506	0·92842	9·72	7·83	0·93368	0·93624	7·70	6·23
16	0·91385	0·91852	10·97	8·83	0·92385	0·92738	8·72	7·05
18	0·90240	0·90864	12·20	9·80	0·91384	0·91856	9·72	7·85
20	0·89069	0·89882	13·38	10·75	0·90364	0·90980	10·70	8·64
22	0·87866	0·88900	14·54	11·66	0·89320	0·90106	11·66	9·40
24	0·86629	0·87918	15·66	12·55	0·88250	0·89230	12·60	10·15
26	0·85353	0·86940	16·74	13·41	0·87152	0·88356	13·52	10·89
28	0·84035	0·85960	17·25	14·24	0·86022	0·87484	14·42	11·60
30	0·82672	0·84976	18·82	15·05	0·84858	0·86610	15·30	12·30
32	0·81259	0·83995	19·80	15·82	0·83657	0·85735	16·16	12·99
34	0·79793	0·83010	20·76	16·57	0·82415	0·84857	17·00	13·65
36	0·78270	0·82021	21·68	17·29	0·81132	0·83979	17·82	14·30
	50°C				75°C			
1	0·99603	0·99602	0·418	0·342	0·99696	0·99696	0·299	0·248
2	0·99206	0·99208	0·834	0·683	0·99393	0·99394	0·597	0·495
4	0·98414	0·98424	1·655	1·354	0·98788	0·98794	1·187	0·984
6	0·97623	0·97646	2·47	2·02	0·98184	0·98196	1·768	1·465
8	0·96831	0·96876	3·26	2·66	0·97581	0·97604	2·34	1·941
10	0·96035	0·96112	4·05	3·30	0·96976	0·97014	2·91	2·41
12	0·95234	0·95352	4·82	3·93	0·96369	0·96432	3·47	2·87
14	0·94426	0·94596	5·58	4·55	0·95759	0·95850	4·02	3·33
16	0·93608	0·93844	6·33	5·15	0·95145	0·95268	4·56	3·78
18	0·92779	0·93098	7·06	5·75	0·94525	0·94692	5·10	4·22
20	0·91938	0·92350	7·78	6·34	0·93899	0·94116	5·63	4·65
22	0·91081	0·91606	8·49	6·91	0·93266	0·93542	6·15	5·08
24	0·90208	0·90866	9·19	7·47	0·92625	0·92972	6·67	5·50
26	0·89316	0·90124	9·88	8·03	0·91973	0·92402	7·17	5·92
28	0·88403	0·89384	10·55	8·57	0·91312	0·91832	7·67	6·33
30	0·87467	0·88644	11·21	9·10	0·90638	0·91260	8·16	6·73
32	0·86507	0·87902	11·86	9·62	0·89952	0·90688	8·65	7·13
34	0·85520	0·87160	12·50	10·13	0·89253	0·90122	9·12	7·52
36	0·84505	0·86417	13·12	10·63	0·88538	0·89550	9·59	7·90
	100°C							
1	0·99766	0·99764	0·221	0·187				
2	0·99532	0·99534	0·442	0·373				
4	0·99066	0·99070	0·881	0·743				
6	0·98601	0·98606	1·317	1·111				
8	0·98137	0·98150	1·751	1·477				
10	0·97678	0·97692	2·18	1·841				
12	0·97207	0·97240	2·61	2·20				
14	0·96740	0·96786	3·04	2·56				
16	0·96272	0·96338	3·46	2·92				
18	0·95801	0·95890	3·89	3·27				
20	0·95327	0·95442	4·31	3·62				
22	0·94849	0·94996	4·72	3·97				
24	0·94367	0·94554	5·13	4·32				
26	0·93880	0·94108	5·55	4·66				
28	0·93388	0·93668	5·96	5·01				
30	0·92889	0·93224	6·36	5·35				
32	0·92383	0·92784	6·77	5·68				
34	0·91871	0·92342	7·17	6·02				
36	0·91350	0·91898	7·57	6·35				

Zelvinskii expressed his data at each temperature by the equation :

$$S = aP - bP^2 \qquad (6)$$

(where S is the solubility in ml. of CO_2 calculated at N.T.P. dissolved in a quantity of water whose volume is 1 ml. at 0°C, and a and b are constants). Since Zelvinskii gives only a limited number of experimental solubilities at the temperatures 0°, 12·43°, 25°, 50°, 75° and 100°C, solubilities at intermediate temperatures are obtained by graphical interpolation of the constants a and b. The accuracy of this procedure, checked against known experimental values, is found to be good within 2%.

Zelvinskii did not measure absorption coefficients at 1 atm.; but these can be obtained by extrapolation of his data at higher pressures, using equation (6). The coefficients obtained by extrapolating to 1 atm. agree with those obtained experimentally by Bohr and Bock, with an average deviation of 2·7% and a maximum of 4·6%.

The absorption coefficients at 25 atm. can be interpolated from Zelvinskii's equations, and compared with the experimental values of Wiebe and Gaddy after correcting their data for the vapour pressure of water. The agreement is within an average deviation of 1·9% and a maximum of 5·7%.

The accuracy of interpolation from Zelvinskii's equations has been checked by comparing interpolated values from equation (6) with actual experimental solubilities determined by him for various pressures [6]. The average deviation was 1%, and the maximum 2·5%.

The data given in the Table for the water-solubility of carbon dioxide have been obtained by interpolation of Zelvinskii's data and a detailed comparison of the results with the data of Wiebe and Gaddy and of Bohr and Bock. It is concluded that the accuracy of these data is better than ± 3%, and in agreement with other published data within the same limits.

Application of Henry's Law

Since the Bohr and Bock data for the absorption coefficients of carbon dioxide in water at 1 atm. are quoted in most textbooks, it was decided to apply Henry's law to these figures and compare the results with values interpolated from the Zelvinskii equations. In view of the maximum deviation deduced in the previous section (better than ± 3%) it appears that deviations of more than 6% between calculated and experimental solubilities at the higher pressures can be considered as deviations for Henry's law. It is evident from the figure that calculations based on this law lead to solubilities consistently higher than the experimental values, the difference increasing as the pressure is raised and the temperature lowered. If 6% is considered as the combined accuracy of the experimental data, Henry's law can be applied only for pressures below *ca.* 5 atm. within the temperature range 0–100°C.

To ascertain whether the non-ideal behaviour of the gas was responsible for the deviations from Henry's law, fugacity was used instead of pressure, again taking the Bohr and Bock experimental data as a basis. The results of the fugacity correction are included in the figure. The effect of using fugacity instead of pressure is to correct Henry's law partially, and to produce

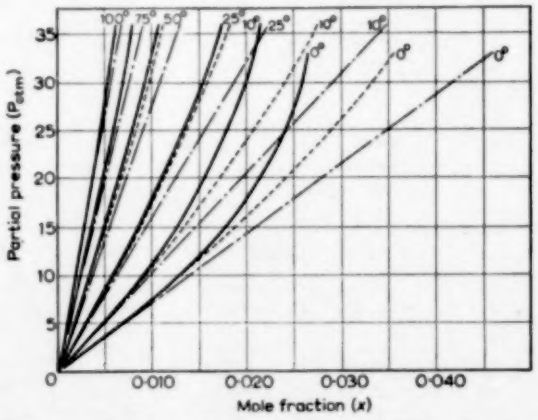

Fig. 1. Comparison of experimental solubilities of carbon dioxide in water with Henry's law and the fugacity correction to Henry's law.

———— Experimental solubility (Zelvinskii).

— · — · — Henry's law based on the absorption coefficients of Bohr and Bock.

— — — — Fugacity correction to Henry's law based on the absorption coefficients of Bohr and Bock.

better agreement with the experimental data. At temperatures between 25° and 100°C, and at all pressures up to 36 atm., the fugacity correction can be applied to the BOHR and BOCK data with an accuracy of better than 6%. At pressures below 10 atm., and at all temperatures between 0° and 100°C, the fugacity correction gives an accuracy better than 6%.

The conclusion reached is that below 25°C and above 10 atm. the system carbon dioxide–water is non-ideal. The deviations cannot be wholly attributed to departure from the ideal gas law, since the fugacity correction to HENRY's law still shows considerable deviations, particularly at low temperatures and high pressures. It must therefore be assumed that the activity coefficients of dissolved carbon dioxide differ considerably from unity. Evidence [10] from the rate of reaction of dissolved carbon dioxide with alkali indicates that less than 1% of it is in the form of carbonic acid, which can therefore contribute little to the deviation of the solution from ideality. Furthermore, temperature affects solubility much more strongly for carbon dioxide than for much less soluble gases such as hydrogen, oxygen, and nitrogen, which obey HENRY's law over a wider range of pressure. This high temperature-coefficient for the decrease in solubility of carbon dioxide shows that the heat of solution is large (relative to that of hydrogen, oxygen, or nitrogen) indicating compound formation between carbon dioxide and water. Carbonic acid being present only in small amount, the nature of such a compound is for the present a matter of conjecture; it may be, for example, that hydrogen bonding between molecular carbon dioxide and water is responsible for the non-ideality of the solutions.

Acknowledgment—The authors thank the Admiralty for permission to publish this paper.

NOTATION

V = volume of one g-mole of gas; litres/g-mole.
P = partial pressure of gas; atm.
T = absolute temperature; °K.
R = universal gas constant; 0·08206 litre, atm./g-mole, °K.
Z = compressibility of gas (PV/RT); dimensionless.
f = fugacity; atm.
α = Bunsen absorption coefficient; volume of gas reduced to N.T.P. dissolved by one volume of water.
x = mol. fraction of dissolved carbon dioxide.
S = solubility in ml of gas (reduced to N.T.P.) dissolved in a quantity of water whose volume is 1 ml at 0°C.
a, b = empirical constants.

REFERENCES

[1] HOUGHTON G., MCLEAN A. M., and RITCHIE P. D. to be published.
[2] BEATTIE J. A. *Proc. Nat. Acad. Sci.* (*Wash.*) 1930 **16** 14.
[3] BEATTIE J. A. and BRIDGEMAN O. C. *Proc. Amer. Acad. Arts Sci.* 1928 **63** 229.
[4] ANDREWS T. *Phil. Trans.* 1876 **166** 421.
[5] MICHELS A. and MICHELS C. *Proc. Roy. Soc.* 1936 **A153** 201.
[6] ZELVINSKII Y. D. *J. Chem. Ind.* (*U.S.S.R.*) 1937 **14** 1250.
[7] WIEBE R. and GADDY V. L. *J. Amer. Chem. Soc.* 1939 **61** 315; 1940 **62** 815.
[8] BOHR C. and BOCK A. *Wied. Ann. Phys.* 1899 (3) **68** 503.
[9] HOLBORN L. and OTTO J. *Z. Phys.* 1924 **23** 77.
[10] KOLTHOFF I. M. and SANDELL E. B. *Textbook of Quantitative Inorganic Analyses*, New York, Macmillan. Revised Ed. 1943 559.

Chemical Engineering Science, 1957, Vol. 6, pp. 138 to 140. Pergamon Press Ltd.

Flooding velocities in packed columns operating at reduced pressures

H. SAWISTOWSKI

Department of Chemical Engineering, Imperial College of Science and Technology, London, S.W.7

(*Received* 30 *October* 1956)

Abstract—The generalized graphical correlation for flooding rates in packed columns presented by LOBO *et al.* [2] can be expressed in the form of an empirical equation as

$$\ln \frac{U_F^2 a}{g \epsilon^3} \frac{\rho_G}{\rho_L} \left(\frac{\mu_L}{\mu_W}\right)^{0.2} = -4 \left(\frac{L}{G}\right)^{\frac{1}{4}} \left(\frac{\rho_G}{\rho_L}\right)^{\frac{1}{4}}.$$

On the basis of this equation it has been shown that in a column operating at reduced pressures flooding will start at the top of the column.

Résumé—L'auteur montre que le calcul des vitesses d'engorgement dans une tour à garnissage par la méthode graphique de LOBO *et al.* peut s'exprimer par nue équation empirique de la forme :

$$\ln \frac{U_F^2 a}{9\epsilon^3} \frac{\rho_G}{\rho_L} \left(\frac{\mu_L}{\mu_W}\right)^{0.2} = -4 \left(\frac{L}{G}\right)^{\frac{1}{4}} \left(\frac{\rho_G}{\rho_L}\right)^{\frac{1}{4}}.$$

Il a montré, à partir de cette équation, que dans une tour à pression réduite, l'engorgement commencera à se produire au sommet de la colonne.

INTRODUCTION

THE usual procedure for determining the flooding velocity in a packed column [1], [3] is to use the graphical correlation prepared by LOBO, FRIEND, HASHMALL and ZENZ [2], which is based on earlier work by SHERWOOD, SHIPLEY and HOLLOWAY [4]. In this correlation a log-log scale is used and the group $\frac{U_F^2 a}{g\epsilon^3} \frac{\rho_G}{\rho_L} \left(\frac{\mu_L}{\mu_W}\right)^{0.2}$ or $\frac{G_F^2 a}{g \epsilon^3 \rho_L \rho_G} \left(\frac{\mu_L}{\mu_W}\right)^{0.2}$ is plotted against $\frac{L}{G} \left(\frac{\rho_G}{\rho_L}\right)^{\frac{1}{2}}$, where

U_F = flooding velocity of the gas phase based on total column cross-section,
G_F = flooding rate expressed as mass flow of the gas phase per unit area of column,
a = surface area of packing per unit volume of column,
g = acceleration due to gravity,
ϵ = void fraction of the packing,
ρ_L = density of the liquid,
ρ_G = density of the gas,
μ_L = viscosity of the liquid,
μ_W = viscosity of water at 20°C (approx. 1 centipoise),
G = mass rate of flow of the gas phase,
L = mass rate of flow of the liquid phase.

In the case of a column operating at reduced pressure the problem is more complicated when the total pressure and the pressure drop are of a similar order of magnitude. The large variations of gas density along the column mean that it is not immediately obvious from the graphical correlation whereabouts in the column flooding will commence. The present paper is an attempt to solve this problem analytically.

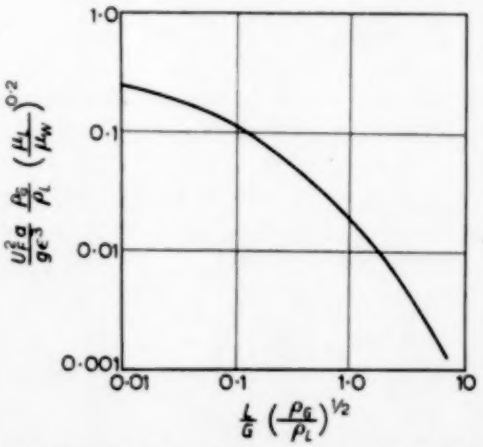

FIG. 1. Generalized correlation for flooding velocities in packed columns [2].

General Expression for Flooding Rates in Packed Columns

The first step is to find an algebraic expression which fits Lobo's graphical correlation. The shape of the curve (Fig. 1) indicates that substitution of a linear scale for logarithmic scale on the abscissa axis might transform the curve into a straight line whose equation would then be of the form :

$$\log \frac{G_F^2\, a}{g\, \epsilon^3\, \rho_L\, \rho_G} \left(\frac{\mu_L}{\mu_W}\right)^{0.2} = -\, C \left[\frac{L}{G}\left(\frac{\rho_G}{\rho_L}\right)^{\frac{1}{2}}\right]^n. \quad (1)$$

For a given column, operating at a constant temperature, we can thus write

$$\log \frac{\rho_G}{A G_F^2} = C \left[\frac{L}{G}\left(\frac{\rho_G}{\rho_L}\right)^{\frac{1}{2}}\right]^n, \quad (2)$$

where $A = \dfrac{a}{g\, \epsilon^3\, \rho_L} \left(\dfrac{\mu_L}{\mu_W}\right)^{0.2} = \text{const.}$

If the experimental data are plotted as $\log\left(\log \dfrac{\rho_G}{A G_F^2}\right)$ versus $\log\left[\dfrac{L}{G}\left(\dfrac{\rho_G}{\rho_L}\right)^{\frac{1}{2}}\right]$, a straight line of slope n will be obtained if equation (1) is applicable, In Fig, 2, it is seen that points which are taken directly from Lobo's curve do in fact lie on a straight line so that the values of C and n can be determined. The flooding rates are, therefore, correlated by the following equation :

$$\log \frac{\rho_G}{A G_F^2} = 1.73 \left[\frac{L}{G}\left(\frac{\rho_G}{\rho_L}\right)^{\frac{1}{2}}\right]^{\frac{1}{4}} \quad (3)$$

or

$$\ln \frac{\rho_G}{A G_F^2} = 4.0 \left[\frac{L}{G}\left(\frac{\rho_G}{\rho_L}\right)^{\frac{1}{2}}\right]^{\frac{1}{4}}. \quad (4)$$

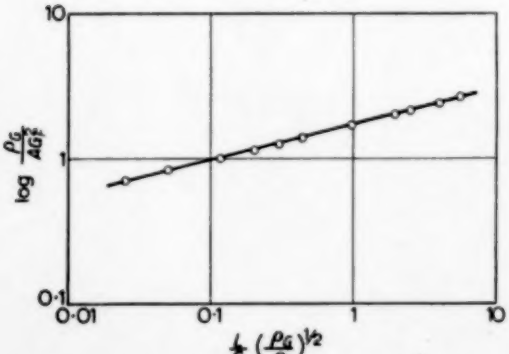

Fig. 2. Evaluation of a general expression for flooding rates in packed columns.

On substituting the value of A, the final expression is

$$\ln \frac{G_F^2\, a}{g\, \epsilon^3\, \rho_L\, \rho_G} \left(\frac{\mu_L}{\mu_W}\right)^{0.2} = -\, 4 \left(\frac{L}{G}\right)^{\frac{1}{4}} \left(\frac{\rho_G}{\rho_L}\right)^{\frac{1}{4}}. \quad (5)$$

The accuracy of this equation is the same as that of the graphical correlation.

Determination of the Position of Critical Flooding Conditions

Equation (4) can be expressed explicitly in G_F^2 as

$$G_F^2 = \frac{\rho_G}{A}\, e^{-B \rho_G^{\frac{1}{4}}}, \quad (6)$$

where $B = 4 \left(\dfrac{L}{G}\right)^{\frac{1}{4}} \rho_L^{-\frac{1}{4}}$.

On differentiation this gives

$$\frac{dG_F^2}{d\rho_G} = \frac{1}{A}\, e^{-B \rho_G^{\frac{1}{4}}} \left(1 - \frac{B \rho_G^{\frac{1}{4}}}{8}\right). \quad (7)$$

Hence, G_F^2 has a maximum or minimum value when $B \rho_G^{\frac{1}{4}} = 8$, i.e. when $\left(\dfrac{L}{G}\right)^{\frac{1}{4}} \left(\dfrac{\rho_G}{\rho_L}\right)^{\frac{1}{4}} = 2$ which is equivalent to $\dfrac{L}{G}\left(\dfrac{\rho_G}{\rho_L}\right)^{\frac{1}{2}} = 16$. As can be seen from Fig. 1 this value of $\dfrac{L}{G}\left(\dfrac{\rho_G}{\rho_L}\right)^{\frac{1}{2}}$ is well outside the possible operating range of packed columns.

Further differentiation of equation (7) leads to the following expression

$$\frac{d}{d\rho_G}\left(\frac{dG_F^2}{d\rho_G}\right) = -\, \frac{B}{64A}\, \rho_G^{-\frac{1}{4}}\, e^{-B \rho_G^{\frac{1}{4}}} (9 - B \rho_G^{\frac{1}{4}}) \quad (8)$$

On substitution of $B \rho_G^{\frac{1}{4}} = 8$ into the above equation it is found that

$$\frac{d^2 (G_F^2)}{d\, \rho_G^2} = -\, \frac{1}{8 A \rho_G}\, e^{-8}. \quad (9)$$

Since the value of the second differential coefficient is negative at $\left(\dfrac{L}{G}\right)^{\frac{1}{4}} \left(\dfrac{\rho_G}{\rho_L}\right)^{\frac{1}{4}} = 2$, the function $G_F^2 = \psi(\rho_G)$ is then a maximum. This maximum is, however, outside the normal operating range so that, in practice, G_F^2 and thus G_F always increases with increasing ρ_G. Hence, in a packed column operated at reduced pressure, flooding would be expected to start at the top of the column where the pressure and therefore the density of the gas phase are lowest. The value

of the flooding rate to be used for design purposes has, thus, to be calculated at the suction pressure of the vacuum pump and not at the pressure existing in the still.

References

[1] Coulson J. M. and Richardson J. F. *Chemical Engineering* Vol. 2, Pergamon Press, London, 1955.

[2] Lobo W. E., Friend L., Hashmall F., and Zenz F. *Trans. Amer. Inst. Chem. Engrs.* 1945 **41** 693.

[3] Sherwood T. K. and Pigford R. L. *Absorption and Extraction* McGraw-Hill, New York, 1952.

[4] Sherwood T. K., Shipley H. G., and Holloway F. A. L. *Ind. Eng. Chem.* 1938 **30** 765.

Letters to the Editors

Discussion of the paper "The partial coefficient of heat-transfer in a drying fluidized bed" by P. M. Heertjes and S. W. McKibbins*

(*Received* 8 *October* 1956)

THE above paper concerns the measurement of heat-transfer coefficients in a fluidized bed of wet silica gel particles. Reference is made to similar work by KETTENRING, MANDERFIELD, and SMITH (*Chem. Eng. Progress* 1950 **46** 139) and to heat transfer from air to coal without drying by WALTON, OLSEN, and LEVENSPIEL (*Ind. Eng. Chem.* 1952 **44** 1474).

Apparently the authors were unaware of the work by the writer and colleague (WAMSLEY and JOHANSON, *Chem. Eng. Progress* 1954 **50** 347) in which heat-transfer coefficients from gas to fluidized solid were obtained using an unsteady-state technique, and in which the results of KETTENRING, MANDERFIELD, and SMITH were extensively discussed.

The heat-transfer coefficients obtained by the unsteady-state technique were only about one-eighth as large as those of KETTENRING, MANDERFIELD and SMITH, or WALTON, OLSEN, and LEVENSPIEL. The data of KETTENRING, MANDERFIELD, and SMITH were reconciled with the unsteady-state data by assuming the solid temperature in the drying experiments was equal to the adiabatic saturation temperature of the incoming air, rather than the temperature used by the authors.

HEERTJES and MCKIBBINS, using an experimental technique developed earlier by HEERTJES, DE BOER, and DE HAAS VAN DORSSER (*Chem. Eng. Sci.* 1953 **2** 97) were able to obtain results seemingly more reliable than those of KETTENRING, MANDERFIELD, and SMITH. The transfer coefficients resulting were stated by the authors (HEERTJES and MCKIBBINS) to differ from those of KETTENRING, *et al.*, and to agree more nearly with those of WALTON *et al.* All three sets of transfer coefficients are of the same magnitude, however, and therefore are about eight times as large as the values found by the unsteady-state technique of WAMSLEY. In view of the increasing industrial applications of the fluidized-bed technique, such a large discrepancy in transfer coefficients must be reconciled, either by further work, or by showing the interpretation of data by one or the other technique to be faulty.

In both researches involving wetted particles, the solid temperature during fluidization was not known. It was assumed equal to the exit gas temperature in each work. The following questions come to mind regarding this assumption:

(a) Why would not the solid temperature approach adiabatic saturation (or wet bulb) temperature in such an adiabatic drying bed? In Fig. 2 of HEERTJES and MCKIBBINS, the temperature of the gel and of exit air is labelled as 15·4°C. The saturation temperature for the inlet air used is about 13°F, or − 10°C.

(b) If solid and gas reach equilibrium temperature within a few millimetres of the bed entrance, why would not the exit air be saturated with moisture at this temperature? In Fig. 11 of HEERTJES, DE BOER, and DE HAAS VAN DORSSER, the exit gas is shown to have a dewpoint of 29·8°F. If this air were in equilibrium with wet solid at a temperature of 12·1°C, as indicated by the authors, its saturation temperature and dewpoint should also be 12·1°C or 53·8°F.

These considerations would seem to indicate that the leaving air is *not* in equilibrium with the wet solid particles. Referring to Fig. 10 of the 1954 paper of WAMSLEY and JOHANSON, it will be noted that WAMSLEY was able to find a finite difference between solid temperature and exit gas temperature, using the same technique for measuring solid temperature employed by HEERTJES and MCKIBBINS. At the conditions of the latter work, this difference would be smaller and more difficult to detect.

It is of importance to note that the major question is not the magnitude of this difference, but rather whether such a difference in solid and gas temperature exists throughout the bed. The existence of even a small driving force throughout the bed, rather than through only the first six millimetres as in Fig. 2 of HEERTJES and MCKIBBINS paper, has a profound effect on the magnitude of the transfer coefficient. Assuming a total bed depth of 60 mm, consistent with HEERTJES's earlier work, the transfer coefficient resulting from the data of Fig. 2 would be decreased about threefold if the solid temperature were 15°C, rather than 15·4°C as assumed.

The above Fig. 2 indicates a large gradient of gas temperature in the bottom of the bed, approaching exit conditions only 6 mm above the bed support. The writer interprets this gradient not as an indication of the rate of heat and mass transfer, but simply as a manifestation of the mixing of inlet gas with the gas already in the bed. The lack of approach to equilibrium of the gas and solid can be attributed to the bypassing of large bubbles or pockets of gas, which do not contact the solid effectively.

University of Washington L. N. JOHANSON
Seattle, Washington, U.S.A.

* *Chem. Eng. Sci.* 1956 **5** 161

Answer by P. M. Heertjes

A POINT-WISE answer to the discussion by L. N. JOHANSON of the paper : The Partial Coefficient of Heat Transfer in a Drying Fluidized Bed (*Chem. Eng. Science* 1956 **5** 161) seems indicated.

(1) The authors were indeed unaware of the work of WAMSLEY and JOHANSON (*Chem. Eng. Progress* 1954 **50** 347), which they regret.

(2) Whether air leaving a wet fluidized mass can reach the adiabatic saturation temperature of the incoming air will depend largely on the water content of the gel. If the water content is such that the water at the surface of the gel behaves as free water and if the apparatus is really adiabatic, the adiabatic saturation temperature of the incoming air will be reached if the bed is high enough, viz. in the experiments presented higher than about 1 cm.

In the experiments under discussion however in the " constant rate " period the water content of the gel was such that the sorbed water does not behave as free water and adsorption phenomena and energies have a strong bearing on the temperature of the leaving air.

It can be found from the data presented that the humidity of the leaving air does not differ more than the experimental error, from the equilibrium humidity of the gel at the temperature of the leaving air (which in our opinion under the conditions given is equal to the gel-temperature). In general it is not correct to use calculated values based on the behaviour of *free* water as the temperature of the gel and it is incorrect in the cases evaluated.

(3) The equations as used by WAMSLEY and JOHANSON will apply for any zone of heat interchange if for A will be taken the real surface of that zone. WAMSLEY and JOHANSON take for A the surface of the whole bed, without giving real proof that this is allowed, e.g., by measuring the air temperatures over the bed. Therefore, the measurements as carried out only give certainty as to the value of the product $h_p A$. If the actual exchanging surface is taken eight times too large, h_p will be found eight times too small. In view of the amount of solid taken, this is quite possible.

(4) As the only proof that the whole surface of the fluidized mass is involved in the heat exchange, WAMSLEY and JOHANSON have measured the temperature of the solid mass, by using the same technique, viz., shutting off the air temporarily, as used by the present writer *et al.* As has been mentioned by the present writer these measurements indicate an equality of gel and leaving air temperature. However it has also been said that the place of such a measurement and moreover the evaluation of the time-temperature curve is very important to decide whether any point of this curve will be near the temperature of the solid mass. In the measurements of WAMSLEY and JOHANSON with non-steady state conditions there can also be a time lag. Moreover, in the cases presented by the present writer *et al.*, other indications have been obtained which show that heat exchange and also mass exchange (not yet published) only occurs over a relatively small zone. These are : equal temperature of the air over the greatest part of the bed, the constant humidity over the same zone, the equality of a mean temperature measured in the bed with comparison of the temperature of the air in this zone.

Some backmixing may occur but the experiments with different amounts of gel, indicate (see *Chem. Eng. Science* 1953 **2** 97) that this influence cannot be large.

(5) In the work of JOHANSON *et al.*, many of the magnitudes used have been calculated based on certain assumptions. In the Delft work material and heat balances could be drawn and checked with measured magnitudes. Including the heat of adsorption (to be found in the literature) besides the heat of evaporation the balances tallied within 5 to 10%.

(6) It may finally be remarked that the coefficient as calculated by the present writer certainly does not represent a correct value, because it has been calculated on a mean porosity over the whole bed. Work is carried out on this topic now.

P. M. HEERTJES

Laboratory for Chemical Engineering of the Delft University Delft

Book reviews

P. C. Carman: Flow of Gases through Porous Media. Butterworths, 1956. 182 pp. 30s.

The flow of gases through porous media is of importance in many operations of interest to the chemical engineer, and Dr. Carman has written a useful monograph on this rapidly developing field. Viscous flow through unconsolidated beds of "normal" or "abnormal" types is first considered in the light of the Kozeny equation, the latter type implying departure of flow behaviour from the equation owing to non-uniform pore texture and high tortuosity. The author then deals with departures from Poiseuille flow when the pore diameter is comparable with or less than the mean free path, and discusses slip and Knudsen flow: with sufficiently fine pores such types of flow are possible at atmospheric pressures. This theme is later developed to include the effects of surface diffusion along the capillary walls; this promises to be a method for isotopic separation. A chapter is devoted to the measurement of surface area by permeability studies, with a very fair discussion of the rival merits of nitrogen adsorption and permeability for this purpose. It should be remembered that for many materials, such as cement or textile fibres, the nitrogen method is less valuable since it gives the total surface, including the internal. There is a short section on gas separation, including chromatography (which most readers would prefer to study in separate monographs), turbulent flow and fluidisation of beds.

The treatment is rather condensed and perhaps could be improved by a more detailed reference to experimental techniques. It is unfortunate that much of the theory is inevitably semi-empirical, which at times gives the reader a feeling of intellectual discomfort. This might have been relieved by a more fundamental discussion of those parts for which a rigorous theory exists, e.g. Knudsen flow. There are some omissions, e.g. Becker's striking work on surface diffusion studies by the use of the field emission microscope.

These, however, are minor criticisms, which probably stem from the author's desire to keep down the size of the monograph. Dr. Carman's writes with authority in a field to which he has contributed many papers, and is to be congratulated on bringing together much recent work on such diverse fields as soil mechanics and molecular sieves. One pleasing feature of a technical book is the use throughout of c.g.s units. The production is good and the price is reasonable.

R. S. Bradley

R. S. Aries and R. D. Newton: Chemical Engineering Cost Estimation. McGraw-Hill Book Company, 1955, pp. 263, $6.00 (45s.).

To present a simple system for arriving at a cost estimate for chemical plant, of sufficient accuracy to enable managerial decisions to be made, seems an impossible aim. This book attempts just that. It is a revised version of the book of the same name in the McGraw-Hill Chemical Engineering Series. No doubt a skilled cost accountant might point out flaws in this book and no doubt the many plots of cost versus capacity for a wide range of unit operations equipment, piping, insulation and so on, represent a gross over simplication. Nevertheless, to the chemical engineer, particularly in the smaller firm, required to produce quickly an estimate of the cost of a projected operation, this book can be recommended as a mine of useful information, clearly presented.

The book is entirely centred on the U.S. market. This means that if a direct conversion of U.S. dollars to local currency is made at a convenient rate of exchange, many of the costs so found will be useless outside of the United States. It is a serious criticism of the book, from the point of view of the European reader, that this problem is completely ignored, and no solution is hinted at. An adidtional chapter on means suggested for convering costs to other currencies should be seriously considered if the book is to be of real use outside of the U.S.A.

D. M. Wilson

Announcement

Symposium on Chemical Reaction Engineering

organized by the

Koninklijk Instituut voor Ingenieurs

and the

Koninklijke Nederlandse Chemische Vereniging

Amsterdam, 7th, 8th and 9th May, 1957

12th Meeting of the

European Federation for Chemical Engineering

PROGRAM

Session I

Introductory papers

General introduction to the Symposium
Prof. Dr. D. W. VAN KREVELEN
(Staatsmijnen in Limburg)

Introduction à la Cinétique des Réactions Chimiques
Prof. M. LETORT
(Centre d'Études et Recherches des Charbonnages de France)

Physical factors in chemical reaction engineering
Prof. Ir. H. KRAMERS
(Technische Hogeschool, Delft)

Session II

Transport phenomena in heterogeneous reactions

Einfluss des Stofftransportes auf den Verlauf heterogener Gasreaktionen
Prof. Dr. E. WICKE
(Universität Hamburg)

Engineering aspects of the oxidation of mercaptans in caustic solutions
Reaction kinetics and design of reactor
Dr. Ir. J. G. VAN DER VUSSE
(Koninklijke/Shell-Laboratorium, Amsterdam)

Gas absorption accompanied by chemical reaction in a wetted wall column
Ir R. A. T. O. NYSING and Prof. Ir H. KRAMERS
(Technische Hogeschool, Delft)

Session III

Nonuniform concentration distribution

The effect of incomplete mixing on homogeneous reactions
Dr. P. V. DANCKWERTS
(United Kingdom Atomic Energy Authority)

Heterogeneous reactions in the liquid phase
Influence of residence time distribution and interaction in the dispersed phase
Dr. K. RIETEMA
(Koninklijke/Shell-Laboratorium, Amsterdam)

Zur Berechnung von Reaktoren für Gemischtphasenreaktionen
Dr. rer. nat. H. HOFMANN
(Technische Hoshschule, Darmstadt)

Session IV

Reactor efficiency and stability

Optimum temperature sequences in reactors
Prof. Dr. K. G. DENBIGH
(University of Edinburgh)

The character of the stationary state of exothermal processes
Dr. C. VAN HEERDEN
(Staatsmijnen in Limburg)

Technological aspects of the catalytic combustion of ammonia with platinum gauze elements
Dr. Ir. A. P. OELE
(Staatsmijnen in Limburg)

Session V

Reactor development

Die Reaktionskinetik bei der Berechnung einiger typischen grosstechnischen Reaktoren
Prof. Dr. K. SCHOENEMANN
(Technische Hochschule, Darmstadt)

Verfahrensmässige Berechnungen des Stoffaustausches gelegentlich der Absorption von Stickstoffoxyden bei der Gewinnung von Salpetersäure
Dipl.-Ing. F. SCHNUR
(Ruhrchemie Aktiengesellschaft, Oberhausen-Holten)